J. Fluid Mech. (2007), *vol.* 583, *pp.* 45–70.
doi:10.1017/S0022112007006106 Printed in the United Kingdom

On hydrodynamic and acoustic modes in a ducted shear flow with wall lining

GREGORY G. VILENSKI† AND SJOERD W. RIENSTRA

Department of Mathematics and Computer Science, Eindhoven University of Technology, PO Box 513, 5600 MB, Eindhoven, The Netherlands

(Received 19 June 2006 and in revised form 1 February 2007)

The propagation of small-amplitude modes in an inviscid but sheared subsonic mean flow inside a duct is considered. For isentropic flow in a circular duct with zero swirl and constant mean flow density the pressure modes are described in terms of the eigenvalue problem for the Pridmore-Brown equation with Myers' locally reacting impedance boundary conditions.

The key purpose of the paper is to extend the results of the numerical study of the spectrum for the case of lined ducts with uniform mean flow in Rienstra (*Wave Motion*, vol. 37, 2003*b*, p. 119), in order to examine the effects of the shear and wall lining. In the present paper this far more difficult situation is dealt with analytically. The high-frequency short-wavelength asymptotic solution of the problem based on the WKB method is derived for the acoustic part of the spectrum. Owing to the stiffness of the governing equations, an accurate numerical study of the spectral properties of the problem for mean flows with strong shear proves to be a non-trivial task which deserves separate consideration.

The second objective of the paper is to gain theoretical insight into the properties of the hydrodynamic part of the spectrum. An analysis of hydrodynamic modes both in the short-wavelength limit and for the case of the narrow duct is presented. For simplicity, only the hard-wall flow configuration is considered.

1. Introduction

The most important source of aircraft noise, at least at take-off, is the turbofan aero-engine. Sound produced by interaction of fan and stator, by interaction of fan with mean flow turbulence, and by the fan alone when its blade tips rotate supersonically, propagates through the inlet and bypass duct of the engine (Eversman 1991). Key features of this noise that need to be addressed in a theoretical study and modelled in any numerical simulation are the relatively high prevailing frequencies (Helmholtz numbers ranging from $\sim$20 for the first harmonic to 70 for the third harmonic), a high subsonic mean flow (Mach numbers during approach and take off ranging between 0.3 and 0.7), a high circumferential wavenumber (relevant periodicities range between, say, 4 to 30), a thin boundary layer in the inlet but sheared flow in the bypass and exhaust duct, and a wall lined with acoustically damping material (usually made of an array of Helmholtz resonator cells) that is mathematically described by a local impedance.

† Present address: School of Mathematics, The University of Manchester, Oxford Road, Manchester, M13 9PL, UK.

Various levels of sophistication in modelling the sound propagation have been published. Analytical or semi-analytical solutions based on modal analysis (also known as normal-mode analysis) are well known and widely applied to cylindrical ducts (circular and annular) of constant cross-section and uniform mean flow, see Zorumski (1974), Chapman (1994) and Rienstra (2003*b*). Ducts of varying cross-section were usually treated numerically, although recently analytical solutions have become available that use the aerodynamically inherent slow variation of the duct diameter (Rienstra 1999, 2003a; Ovenden 2005; Mattheij, Rienstra & ten Thije Boonkkamp 2005). Modal analysis has been studied for ducts of constant cross-section and shear or swirling flow, for example in Golubev & Atassi (1998), Tam & Auriault (1998), Kousen (1999), Nijboer (2001) and Cooper & Peake (2005), with generalizations to slowly varying ducts in Cooper & Peake (2001).

In the present paper we aim to further our knowledge of modes in circular and annular ducts with strictly subsonic sheared flow with particular emphasis on the role of lined walls. The paper will be of analytic nature, supported by numerical results of a companion paper (Vilenski & Rienstra 2006) on the numerical treatment of the problem.

An important aspect of the small-amplitude perturbation techniques employed for the description of the wave dynamics in such flows is the behaviour of the spectrum of the related linearized equations of motion. Of special theoretical interest here is the high-frequency limit, since it is important for aero-engine flows and also presents considerable difficulty for direct numerical treatment, owing to the stiffness of the governing equations.

The dispersion relation of the compressible linearized Euler equations is known to have two branches. The first branch corresponds to acoustic waves. The second branch, which is usually ignored when we are only interested in acoustic behaviour, is associated with the waves that do not propagate along fluid particles, but remain stationary with respect to the fluid. Traditionally, waves of this type are studied in the context of hydrodynamic stability theory and are called convected or hydrodynamic waves. For compressible two-dimensional flows the theory of these waves was given in 1946 in the classical work by Lees & Lin (1946) who used a modal approach.

Lees & Lin (1946) considered temporal stability of a non-uniform unbounded parallel flow, with the amplitudes of the perturbation waves being functions of the cross-stream variable. They also studied the limit of vanishing viscosity and obtained the compressible analogue of Rayleigh's equation for the amplitude of the pressure mode, also known as the two-dimensional Pridmore–Brown equation in the aeroacoustic literature. They examined in detail the solution's behaviour in the vicinity of the critical layer, where the phase speed of the mode is equal to the local mean flow velocity and obtained the generalization of the inflection point theorem. Further discussion of their theory and other related results can be found in Criminale, Jackson & Josine (2003) and Schlichting *et al.* (2000).

In the modal approach both types of waves have to be studied within the same set of governing equations. They can be reduced to a single second-order ordinary differential equation, say, for the pressure amplitude P. For a homentropic non-swirling vortical flow in a circular duct this is the Pridmore–Brown equation (3.1), and equation (2.24) for a general axisymmetric ducted flow with swirl and shear. Together with appropriate boundary conditions, either of these equations leads to an eigenvalue problem, where the spectral parameter (non-dimensional wavenumber $\widetilde{k}$ in the present case) appears in the coefficients before different derivatives of the differential equation and, possibly, in the boundary conditions. This is the opposite of

the Sturm–Liouville problem, where the spectral parameter enters the problem linearly only via the coefficient before the zeroth derivative of the governing differential equation. However, as in the Sturm–Liouville case, (see Naimark 1969 for details), in the domain D of the complex plane $\widetilde{k}$, where the coefficients of the equation (3.1) (or (2.24), respectively) and the coefficients of the corresponding boundary conditions are analytic functions, the related eigenvalue problem cannot have more than countable number of eigenvalues, and these eigenvalues cannot have a finite limiting point in this domain. The number of linearly independent eigensolutions corresponding to a given eigenvalue is called the eigenvalue's multiplicity. Since a second-order ordinary differential equation cannot have more than two linearly independent solutions, the multiplicity of the eigenvalues cannot be greater than two. In the domain D the Green's function of the related differential operator is meromorphic, with the eigenvalues being its poles of order not greater than two.

However, in the regions of the complex wavenumber plane $\widetilde{k}$, where the phase velocity of the mode is equal to the mean flow velocity, the coefficients of the modal differential equation are not analytic. Such wavenumbers may potentially correspond to convected modes. Although the spectral theory for singular Sturm–Liouville operators is well known (Stakgold 1998), to the authors' knowledge, its generalization to the case of equations with non-analytic coefficients discussed in the previous paragraph is not available. As a result, only limited data on the properties of the spectrum of such equations currently exist in the literature and only for relatively small values of the Helmholtz number. In particular, coverage of the properties of the hydrodynamic part of the spectrum, in our view, remains insufficient.

The aim of this work is to revisit the problem of the propagation of small disturbances in an annular duct with sheared mean flow and wall lining in order to shed some extra light on these issues. We also aim to study the influence of the wall lining on the spectrum structure, assuming the validity of the Ingard–Myers condition as a limiting no-slip model for mean flow velocity profiles with strong near-wall shear.

An important aspect of sound propagation in a non-dissipative medium is its direction, also known as the problem of causality. It is not directly clear whether a duct mode travels to the right or to the left. In time-harmonic problems this can usually be resolved by giving the medium artificially slight dissipation in the form of a small complex part of the frequency. If the mean flow is moving, however, the disturbances may be unstable and a small complex part is not enough, making a deeper causality analysis necessary. In the present problem we mainly consider a mean flow that slips along the lined wall. This appears to be a much more difficult configuration in terms of stability and causality than one might expect (Rienstra & Tester 2005; Rienstra 2006; Brambley & Peake 2006). Therefore, we decided to leave any issue of causality outside the present analysis.

The analysis is based on an asymptotic approach of the WKB type similar to what has been proposed by Envia (1998) and Cooper & Peake (2001). The WKB solution is extended to the case of soft walls and is used to predict analytically typical behaviour of the axial wavenumber in the complex plane when the wall impedance varies in the complex plane. The properties of the hydrodynamic part of the spectrum for the sheared mean flow without swirl (i.e. the Pridmore–Brown equation, Pridmore–Brown 1958) are also studied analytically.

The paper is composed of four sections. In § 2 we deal with the general aspects of modal analysis, our aim being to recall the main aspects of the generic problem with the swirl and shear and provide a consistent derivation of the governing equation for

the case of mean flow with shear only in the light of the basic principles. In view of recent advances in the analysis of swirling flows (Golubev & Atassi 1998; Tam & Auriault 1998; Nijboer 2001; Kousen 1999; Cooper & Peake 2005), it was important to bring together essential information about the structure of the modal equation for flows with swirl and shear, and for flows with shear only, which is studied in the present paper. This applies particularly to the difference in the nature of the singularity in the differential operators (2.24) and (2.28) which govern these two problems.

In the introduction to § 3 and § 3.1 the WKB approach is used to derive the dispersion relation for the case of impedance walls in the absence of (radial) turning points in the flow region. Sections 3.1.1 and 3.1.2 consider hard walls only and deal mainly with the practical aspect of the WKB analysis. Here the comparison of the accuracy of the WKB prediction with the known exact solution for the case of uniform flow is made. The most important aspect of this is the exceptionally high quality of the WKB approximation even for moderate wavenumbers and frequencies. In the high-frequency range the WKB solution was found to rival numerical computations (for details see Vilenski & Rienstra 2006). There has been a demand for such tool in our recent work with the industry. Detailed examination of many numerical methods now available for the purposes of modal analysis shows that it is always possible that some eigenvalues can be missed and it is hard to make the numerical results accurate, particularly with regard to high frequencies and the hydrodynamic part of the spectrum.

The results of §§ 3.1.1 and 3.1.2 are also needed for the analysis in §§ 3.1.3 and 3.1.4, in which we describe the role of shear and lining in the cut-off part of the spectrum and the surface modes. Although the cut-off part of the spectrum is relatively unimportant for the propagation problem, knowledge of a large number of cut-off modes is sometimes needed in applications. One such example is the problem of extraction of the acoustic pressure field from a large-scale CFD computation near the fan region for the purpose of further aeroacoustic computations (see Ovenden & Rienstra 2004). In such a case the detailed *a priori* knowledge of the spectral properties of the problem is very useful. In fact we have written this work with the need for an analytic approach to the complicated practical situations of this type in mind (see Vilenski 2006). This also explains why much care is taken to ensure that the proposed asymptotic results give sufficiently accurate representation of the available exact solutions.

Section 3.2 is dedicated to the analysis of turning points (i.e. the change from oscillatory to exponential behaviour in the radial direction) of the mode, both for ducts with hard walls and with lining. Section 3.3 deals with the hydrodynamic part of the spectrum. For simplicity, we have restricted consideration to the hard-wall boundary conditions. The section examines the smoothness properties of hydrodynamic modes and establishes their connection with the properties of the Green's function. Section 4 contains the conclusions.

2. Problem formulation and governing equations

Consider an inviscid non-heat-conducting compressible perfect gas flow inside an infinitely long straight annular duct of inner radius h and outer radius d (see figure 1). Let x, r and θ be the axial, radial and circumferential coordinates, u, v and w the projections of the velocity vector on the coordinate axes x, r and θ respectively, ρ and p the density and the pressure. The dimensional equations for conservation of

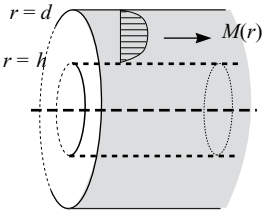

FIGURE 1. Flow geometry.

mass, and radial, circumferential and axial components of momentum and energy are

$$\frac{\partial \rho}{\partial t} + \frac{1}{r}\frac{\partial (r\rho v)}{\partial r} + \frac{1}{r}\frac{\partial (\rho w)}{\partial \theta} + \frac{\partial (\rho u)}{\partial x} = 0, \tag{2.1}$$

$$\rho\left(\frac{\partial v}{\partial t} + v\frac{\partial v}{\partial r} + \frac{w}{r}\frac{\partial v}{\partial \theta} + u\frac{\partial v}{\partial x} - \frac{w^2}{r}\right) = -\frac{\partial p}{\partial r}, \tag{2.2}$$

$$\rho\left(\frac{\partial w}{\partial t} + v\frac{\partial w}{\partial r} + \frac{w}{r}\frac{\partial w}{\partial \theta} + u\frac{\partial w}{\partial x} + \frac{vw}{r}\right) = -\frac{1}{r}\frac{\partial p}{\partial \theta}, \tag{2.3}$$

$$\rho\left(\frac{\partial u}{\partial t} + v\frac{\partial u}{\partial r} + \frac{w}{r}\frac{\partial u}{\partial \theta} + u\frac{\partial u}{\partial x}\right) = -\frac{\partial p}{\partial x}, \tag{2.4}$$

$$\frac{\partial p}{\partial t} + v\frac{\partial p}{\partial r} + \frac{w}{r}\frac{\partial p}{\partial \theta} + u\frac{\partial p}{\partial x} + \gamma p\left(\frac{1}{r}\frac{\partial (rv)}{\partial r} + \frac{1}{r}\frac{\partial w}{\partial \theta} + \frac{\partial u}{\partial x}\right) = 0. \tag{2.5}$$

Here t is time, $\gamma = c_p/c_v$ is the ratio of specific heat capacities at constant pressure and constant volume, respectively. The pressure, the density and the absolute temperature T satisfy the equation of state $p = R\rho T$, $R = c_p - c_v$.

Assume that the total flow field is the sum of a mean flow and small-amplitude unsteady perturbations

$$(u, v, w, \rho, p) = (\bar{u}, \bar{v}, \bar{w}, \bar{\rho}, \bar{p}) + (\tilde{u}, \tilde{v}, \tilde{w}, \tilde{\rho}, \tilde{p}). \tag{2.6}$$

The mean flow is independent of x, its radial velocity is zero, and its circumferential velocity is also independent of θ, i.e.

$$\frac{\partial}{\partial x} \equiv 0, \quad \bar{\boldsymbol{v}} = 0, \quad \frac{\partial \bar{w}}{\partial \theta} = 0.$$

In this case the mean flow is governed by the following well-known solution (see for instance Tam & Auriault 1998):

$$\bar{\rho} = \bar{\rho}(r), \quad \bar{w} = \bar{w}(r), \quad \bar{u} = \bar{u}(r), \quad p = p_d - \int_r^d \bar{\rho}(\xi)\frac{\bar{w}^2(\xi)}{\xi}\,\mathrm{d}\xi, \tag{2.7}$$

where constant p_d is the pressure at $r = d$, $\bar{\rho}(r)$, $\bar{w}(r)$ are arbitrary functions of r, and $\bar{u}$ is an arbitrary function of its arguments.

All three vorticity components in the x-, θ- and r-direction are non-zero for the mean flow (2.7) and are equal to

$$\frac{1}{r}\frac{\mathrm{d}(r\bar{w})}{\mathrm{d}r}, \quad -\frac{\partial \bar{u}}{\partial r}, \quad \frac{1}{r}\frac{\partial \bar{u}}{\partial \theta},$$

respectively.

The small-amplitude disturbance field is governed by the linearized Euler equations

$$\frac{\partial\widetilde{\rho}}{\partial t}+\bar{u}\frac{\partial\widetilde{\rho}}{\partial x}+\frac{1}{r}\frac{\partial(r\bar{\rho}\widetilde{v})}{\partial r}+\frac{\bar{w}}{r}\frac{\partial\widetilde{\rho}}{\partial\theta}+\bar{\rho}\left(\frac{1}{r}\frac{\partial\widetilde{w}}{\partial\theta}+\frac{\partial\widetilde{u}}{\partial x}\right)=0, \tag{2.8}$$

$$\bar{\rho}\left(\frac{\partial\widetilde{v}}{\partial t}+\bar{u}\frac{\partial\widetilde{v}}{\partial x}+\frac{\bar{w}}{r}\frac{\partial\widetilde{v}}{\partial\theta}-\frac{2\bar{w}}{r}\widetilde{w}\right)-\frac{\bar{w}^2}{r}\widetilde{\rho}=-\frac{\partial\widetilde{p}}{\partial r}, \tag{2.9}$$

$$\bar{\rho}\left(\frac{\partial\widetilde{w}}{\partial t}+\bar{u}\frac{\partial\widetilde{w}}{\partial x}+\frac{\bar{w}}{r}\frac{\partial\widetilde{w}}{\partial\theta}+\frac{\mathrm{d}\bar{w}}{\mathrm{d}r}\widetilde{v}+\frac{\bar{w}}{r}\widetilde{v}\right)=-\frac{\partial\widetilde{p}}{\partial\theta}, \tag{2.10}$$

$$\bar{\rho}\left(\frac{\partial\widetilde{u}}{\partial t}+\bar{u}\frac{\partial\widetilde{u}}{\partial x}+\frac{\bar{w}}{r}\frac{\partial\widetilde{u}}{\partial\theta}+\frac{\partial\bar{u}}{\partial r}\widetilde{v}+\frac{\partial\bar{u}}{\partial\theta}\frac{\widetilde{w}}{r}\right)=-\frac{\partial\widetilde{p}}{\partial x}, \tag{2.11}$$

$$\frac{\partial\widetilde{p}}{\partial t}+\bar{u}\frac{\partial\widetilde{p}}{\partial x}+\frac{\bar{w}}{r}\frac{\partial\widetilde{p}}{\partial\theta}+\frac{\bar{\rho}\bar{w}^2}{r}\widetilde{v}+\gamma\bar{p}\left(\frac{1}{r}\frac{\partial(r\widetilde{v})}{\partial r}+\frac{1}{r}\frac{\partial\widetilde{w}}{\partial\theta}+\frac{\partial\widetilde{u}}{\partial x}\right)=0. \tag{2.12}$$

If the resulting small-amplitude disturbances are sought in the form

$$(\widetilde{u},\widetilde{v},\widetilde{w},\widetilde{\rho},\widetilde{p})=(U,V,W,R,P)\exp(-\mathrm{i}\omega t+\mathrm{i}kx+\mathrm{i}m\theta), \tag{2.13}$$

where ω is the excitation frequency, and k and m are the axial and the circumferential wavenumbers, respectively, then the amplitudes (U, V, W, R, P) which are unknown functions of r satisfy the system of equations

$$\mathrm{i}\lambda R+\frac{1}{r}\frac{\mathrm{d}(r\bar{\rho}V)}{\mathrm{d}r}+\bar{\rho}\left(\frac{\mathrm{i}m}{r}W+\mathrm{i}kU\right)=0, \tag{2.14}$$

$$\bar{\rho}\left(\mathrm{i}\lambda V-\frac{2\bar{w}}{r}W\right)-\frac{\bar{w}^2}{r}R=-P', \tag{2.15}$$

$$\mathrm{i}\lambda\bar{\rho}W+\bar{\rho}\left(\bar{w}'+\frac{\bar{w}}{r}\right)V=-\frac{\mathrm{i}m}{r}P, \tag{2.16}$$

$$\bar{\rho}(\mathrm{i}\lambda U+\bar{u}'V)=-\mathrm{i}kP, \tag{2.17}$$

$$\mathrm{i}\lambda P+\frac{\bar{\rho}\bar{w}^2}{r}V+\gamma\bar{p}\left(\frac{1}{r}\frac{\mathrm{d}(rV)}{\mathrm{d}r}+\frac{im}{r}W+\mathrm{i}kU\right)=0, \tag{2.18}$$

while λ, given by

$$\lambda=-\omega+k\bar{u}+m\bar{w}/r,$$

is the eigenvalue of the operator $-\mathrm{i}(\partial_t+\bar{u}\partial_x+\bar{w}r^{-1}\partial_\theta)$. Here and in what follows the primes denote differentiation with respect to r. In order to reduce system (2.14–2.18) to a single equation for P, we first eliminate U and W. This can be achieved by eliminating W from (2.15) and (2.16), $\mathrm{i}mr^{-1}W+\mathrm{i}kU$ from (2.14) and (2.18), expressing the latter sum via (2.16) and (2.17) and substituting it into (2.14):

$$\mathrm{i}\lambda\bar{\rho}P-\mathrm{i}\lambda\gamma\bar{p}R+\left(\frac{\bar{w}^2}{r}\bar{\rho}^2-\gamma\bar{\rho}'\bar{p}\right)V=0, \tag{2.19}$$

$$\frac{2\mathrm{i}m\bar{w}}{r^2}P-\frac{\mathrm{i}\lambda\bar{w}^2}{r}R+\bar{\rho}\left(\frac{2\bar{w}}{r}\left(\bar{w}'+\frac{\bar{w}}{r}\right)-\lambda^2\right)V=-\mathrm{i}\lambda P', \tag{2.20}$$

$$-\lambda^2R+\frac{\mathrm{i}\lambda}{r}\frac{\mathrm{d}(r\bar{\rho}V)}{\mathrm{d}r}+\left(\frac{m^2}{r^2}+k^2\right)P-\mathrm{i}\bar{\rho}\left(\frac{m}{r}\left(\bar{w}'+\frac{\bar{w}}{r}\right)+k\bar{u}'\right)V=0. \tag{2.21}$$

Eliminating R from (2.20) and (2.21) via (2.19) yields the system for the pressure and radial velocity amplitudes

$$\mathrm{i}\lambda P' + \mathrm{i}BP - AV\bar{\rho} = 0, \tag{2.22}$$

$$\frac{1}{r}\frac{\mathrm{d}(rV)}{\mathrm{d}r} + \frac{\mathrm{i}\Omega}{\bar{\rho}\lambda}P + CV = 0. \tag{2.23}$$

Here

$$A = \lambda^2 + \frac{\bar{w}^4}{\bar{c}^2 r^2} - \frac{\bar{w}^2}{r}\frac{\bar{\rho}'}{\bar{\rho}} - \frac{2\bar{w}}{r}\left(\bar{w}' + \frac{\bar{w}}{r}\right), \quad B = \frac{2m\bar{w}}{r^2} - \frac{\lambda\bar{w}^2}{\bar{c}^2 r},$$

$$C = \frac{\bar{w}^2}{\bar{c}^2 r} - \frac{1}{\lambda}\left(\frac{m}{r}\left(\bar{w}' + \frac{\bar{w}}{r}\right) + k\bar{u}'\right), \quad \Omega = \frac{\lambda^2}{\bar{c}^2} - k^2 - \frac{m^2}{r^2}, \quad \bar{c}^2 = \frac{\gamma\bar{p}}{\bar{\rho}}.$$

System (2.22)–(2.23) coincides with the related system of equations obtained by Nijboer (2001). Elimination of V leads to a single differential equation for the pressure amplitude P:

$$P'' + \left(\frac{\lambda + Br}{\lambda r} + C + \frac{\bar{\rho}A}{\lambda}\frac{\mathrm{d}}{\mathrm{d}r}\left(\frac{\lambda}{\bar{\rho}A}\right)\right)P' + \left(\frac{A\Omega}{\lambda^2} + \frac{\bar{\rho}A}{\lambda r}\frac{\mathrm{d}}{\mathrm{d}r}\left(\frac{Br}{\bar{\rho}A}\right) + \frac{BC}{\lambda}\right)P = 0. \tag{2.24}$$

In order to state boundary conditions for this equation, assume that the duct walls are treated with locally reacting lining with the complex specific impedances Z_h and Z_d for $r = h$ and $r = d$, respectively. Here $r = d$ is the exterior radius of the duct and $r = h$ is the inner radius (see figure 1). According to Ingard (1959) and Myers (1980), the following relations must be satisfied at the duct walls to correct for the vanishing mean-flow boundary layer:

$$-\mathrm{i}\omega\tilde{v}_n = \left(-\mathrm{i}\omega + \bar{u}\frac{\partial}{\partial x} + \frac{\bar{w}}{r}\frac{\partial}{\partial\theta}\right)\left(\frac{\tilde{p}}{Z}\right), \tag{2.25}$$

where $\tilde{v}_n$ is the projection of the perturbation velocity on the outwardly directed normal to the duct wall ($\tilde{v}_n = \tilde{v}$ for $r = d$ and $\tilde{v}_n = -\tilde{v}$ for $r = h$), and $Z = Z_d$ or $Z = Z_h$ for $r = d$ or $r = h$, respectively. Substitution of (2.13) in (2.25) together with (2.22) gives the required boundary conditions for the equation (2.24):

$$P' + \left(\frac{B}{\lambda} + \frac{\mathrm{i}\bar{\rho}A}{\omega Z_h}\right)P = 0 \quad \text{on } r = h, \tag{2.26}$$

$$P' + \left(\frac{B}{\lambda} - \frac{\mathrm{i}\bar{\rho}A}{\omega Z_d}\right)P = 0 \quad \text{on } r = d. \tag{2.27}$$

The hard-wall boundary condition on either of the walls is recovered in the limit Z_h or $Z_d \to \infty$.

In the eigenvalue problem (2.24), (2.26), (2.27) the excitation frequency ω and the circumferential wavenumber m are given real numbers while the axial complex wavenumber k is an unknown spectral parameter.

Further discussion of the modal analysis for swirling flows can be found in Golubev & Atassi (1998), Tam & Auriault (1998), Kousen (1999), Nijboer (2001) and Cooper & Peake (2005), etc. However, the main interest here will be in the situation of zero mean circumferential velocity $\bar{w} = 0$ and constant mean flow density $\bar{\rho}$ (and hence pressure $\bar{p}$), in which case (2.24) reduces to the Pridmore-Brown equation

$$P'' + \beta(r)P' + \gamma(r)P = 0, \tag{2.28}$$

where

$$\beta(r) = \frac{1}{r} + \frac{2k\bar{u}'}{\omega - k\bar{u}}, \quad \gamma(r) = \frac{(\omega - k\bar{u})^2}{c_0^2} - k^2 - \frac{m^2}{r^2} \quad \text{and} \quad c_0^2 = \frac{\gamma \bar{p}}{\bar{\rho}}.$$

In this case the boundary conditions are

$$P' + \frac{\mathrm{i}\bar{\rho}(\omega - k\bar{u})^2}{\omega Z_h} P = 0 \quad \text{on } r = h, \tag{2.29}$$

$$P' - \frac{\mathrm{i}\bar{\rho}(\omega - k\bar{u})^2}{\omega Z_d} P = 0 \quad \text{on } r = d. \tag{2.30}$$

In the present work we study the solutions of field equation (2.28) with various versions of conditions (2.29), (2.30). Any properties of the impedance as a function of frequency will not be specified since we will not comment on the issue of causality.

3. Asymptotic analysis

The following non-dimensional quantities will be used in this section:

$$\widetilde{\omega} = \omega d/c_0, \quad \widetilde{k} = kd, \quad z_h = Z_h/\bar{\rho}c_0, \quad z_d = Z_d/\bar{\rho}c_0,$$
$$M = \bar{u}/c_0, \quad M_h = \bar{u}(h)/c_0, \quad M_d = \bar{u}(d)/c_0, \quad s = h/d.$$

Also assume that the pressure amplitude P is scaled by (now constant) $\bar{\rho}c_0^2$, time by d/c_0, velocities by the sound speed c_0, and r and other distances by d, so that the problem (2.28)–(2.30) can be rewritten in the following non-dimensional form:

$$P'' + \left(\frac{1}{r} + \frac{2\widetilde{k}M'}{\widetilde{\omega} - \widetilde{k}M}\right)P' + \left((\widetilde{\omega} - \widetilde{k}M)^2 - \widetilde{k}^2 - \frac{m^2}{r^2}\right)P = 0, \tag{3.1}$$

$$P' + \frac{\mathrm{i}(\widetilde{\omega} - \widetilde{k}M_h)^2}{\widetilde{\omega} z_h} P = 0 \quad \text{on } r = s, \tag{3.2}$$

$$P' - \frac{\mathrm{i}(\widetilde{\omega} - \widetilde{k}M_d)^2}{\widetilde{\omega} z_d} P = 0 \quad \text{on } r = 1. \tag{3.3}$$

In order to reduce the system (3.1)–(3.3) to a form convenient for WKB analysis, introduce the new independent variable $\tau = \tau(r)$ which will be specified in what follows and the new dependent variable $w(\tau)$ (not to be confused with the total circumferential velocity w in § 2) such that

$$P = \frac{\alpha(r) w(\tau)}{(\tau')^{1/2}}, \quad \alpha(r) = \frac{\widetilde{\omega} - \widetilde{k}M}{\sqrt{r}}, \tag{3.4}$$

where τ' denotes derivative with respect to r and, hence,

$$P' = \alpha(r)\left[(\tau')^{1/2}\frac{\mathrm{d}w}{\mathrm{d}\tau} - \frac{\tau'' w}{2(\tau')^{3/2}}\right] + \frac{\mathrm{d}\alpha}{\mathrm{d}r}\frac{w}{(\tau')^{1/2}}.$$

τ will be suitably chosen later. The system (3.1)–(3.3) then takes the form

$$\frac{\mathrm{d}^2 w}{\mathrm{d}\tau^2} + \left\{\frac{q}{(\tau')^2} - \frac{\tau'''}{2(\tau')^3} + \frac{3(\tau'')^2}{4(\tau')^4}\right\} w = 0, \tag{3.5}$$

$$\frac{\mathrm{d}w}{\mathrm{d}\tau} + \left\{-\frac{\tau''}{2\tau'} + \frac{\alpha'(s)}{\alpha(s)} + \frac{\mathrm{i}(\widetilde{\omega} - \widetilde{k}M_h)^2}{\widetilde{\omega} z_h}\right\}\frac{w}{\tau'} = 0 \quad \text{at} \quad \tau = \tau(s), \tag{3.6}$$

$$\frac{\mathrm{d}w}{\mathrm{d}\tau}+\left\{-\frac{\tau''}{2\tau'}+\frac{\alpha'(1)}{\alpha(1)}-\frac{\mathrm{i}(\widetilde{\omega}-\widetilde{k}M_d)^2}{\widetilde{\omega}z_d}\right\}\frac{w}{\tau'}=0 \quad \text{at} \quad \tau=\tau(1), \tag{3.7}$$

where

$$q(r)=(\widetilde{\omega}-\widetilde{k}M)^2-\widetilde{k}^2-\frac{m^2}{r^2}-\frac{2\widetilde{k}^2(M')^2}{(\widetilde{\omega}-\widetilde{k}M)^2}-\frac{\widetilde{k}(M''+M'/r)}{\widetilde{\omega}-\widetilde{k}M}+\frac{1}{4r^2}. \tag{3.8}$$

It is assumed in this section that the duct is not circular ($s>0$), the spectral parameter $\widetilde{k}$ is large and, unless specified otherwise, the frequency $\widetilde{\omega}$ and the circumferential wavenumber m are of the same order of magnitude as $\widetilde{k}$. It follows from (3.8) that $q(r)=O(\widetilde{k}^2)$ as $\widetilde{k}\to\infty$. The exceptions are the vicinities of turning points say $r=r_*$, where $q(r_*)=0$ and the vicinities of the points where $\widetilde{\omega}-\widetilde{k}M$ goes to zero (Cooper & Peake 2001). According to the WKB methodology (see for instance Barantsev & Engelgart 1987), away from these points the main-order part of the operator on the left-hand side of (3.5) can be extracted by choosing $\tau'(r)=q^{1/2}$. In this case the first term in the curly brackets is equal to one whereas the remaining terms are $O(\widetilde{k}^{-2})$ and can be neglected in the main-order analysis. The case of one turning point can be dealt with by taking $\tau'(r)=(q/\tau)^{1/2}$. The first term in the curly brackets in (3.5) is then equal to $\tau=O(\widetilde{k}^{2/3})$, with the other two terms being $O(\widetilde{k}^{-2/3})$ uniformly in r, if $\widetilde{\omega}-\widetilde{k}M\neq 0$. The case of $\widetilde{\omega}-\widetilde{k}M=0$ will be studied separately. Although physically possible, the situation of multiple turning points will not be considered in the present study.

3.1. *Ordinary WKB approximation*

Assume that $\widetilde{\omega}$, m and $\widetilde{k}$ are such that neither $q(r)$ nor $\widetilde{\omega}-\widetilde{k}M(r)$ tend to zero for $s\leqslant r\leqslant 1$ and choose

$$\tau(r)=\int_s^r\sqrt{q(\xi)}\,\mathrm{d}\xi, \quad \tau_d=\tau(1)\equiv\int_s^1\sqrt{q(\xi)}\,\mathrm{d}\xi.$$

The aim of this section is to study the influence of the wall impedance on the properties of the spectrum of the problem (3.1)–(3.3). For this reason, we assume here that the impedance terms in (3.6), (3.7) are large compared to unity, i.e.

$$\frac{(\widetilde{\omega}-\widetilde{k}M)^2}{\widetilde{\omega}z}\gg 1 \tag{3.9}$$

for $z=z_h, z_d$. If the opposite is true, the resulting leading-order problem is governed by the hard-wall solution derived in the following subsection. The physical meaning of (3.9) is that the wall impedance z does not go to the hard-wall limit $z=\infty$ too rapidly as $\widetilde{k}$ increases. The problem (3.5)–(3.7) then becomes

$$\frac{\mathrm{d}^2w}{\mathrm{d}\tau^2}+w=0, \quad \frac{\mathrm{d}w}{\mathrm{d}\tau}+\mathrm{i}\sigma_h w=0 \quad \text{at} \quad \tau=0, \quad \frac{\mathrm{d}w}{\mathrm{d}\tau}-\mathrm{i}\sigma_d w=0 \quad \text{at} \quad \tau=\tau_d, \tag{3.10}$$

where

$$\sigma_h=\frac{(\widetilde{\omega}-\widetilde{k}M_h)^2}{\widetilde{\omega}z_h\tau'(s)}, \quad \sigma_d=\frac{(\widetilde{\omega}-\widetilde{k}M_d)^2}{\widetilde{\omega}z_d\tau'(1)}. \tag{3.11}$$

It has non-zero solution $w=\cos(\tau)-\mathrm{i}\sigma_h\sin(\tau)$ if the spectral parameter $\widetilde{k}$ satisfies the equation

$$\mathrm{e}^{\mathrm{i}2\tau_d}=\frac{(1+\sigma_h)(1+\sigma_d)}{(1-\sigma_h)(1-\sigma_d)}. \tag{3.12}$$

WKB $\widetilde{k}$	Exact $\widetilde{k}$	Relative error %
$16.67 + \mathrm{i} \cdot 11.69$	$16.67 + \mathrm{i} \cdot 12.11$	3.60
$16.67 + \mathrm{i} \cdot 26.62$	$16.67 + \mathrm{i} \cdot 26.73$	0.41
$16.67 + \mathrm{i} \cdot 38.04$	$16.67 + \mathrm{i} \cdot 38.10$	0.16
$16.67 + \mathrm{i} \cdot 48.49$	$16.67 + \mathrm{i} \cdot 48.53$	0.082
$16.67 + \mathrm{i} \cdot 58.48$	$16.67 + \mathrm{i} \cdot 58.51$	0.051

TABLE 1. Ordinary WKB approximation versus exact solution: $\widetilde{\omega} = 25$, $m = 15$, $s = 0.6$, $M = 0.5$.

If the restriction (3.9) is violated either for $r = s$ or $r = 1$, then $\sigma_h = o(1)$ or $\sigma_d = o(1)$, respectively, and the related hard-wall boundary condition is recovered. Our next step is to consider the hard-wall limit.

3.1.1. *The hard-wall solution*

For the duct with hard walls, $\sigma_h = \sigma_d = 0$, the dispersion relation (3.12) reduces to the following equation for $\widetilde{k}$:

$$\int_s^1 \sqrt{q(\xi)}\,\mathrm{d}\xi = n\pi, \tag{3.13}$$

where n is an integer (cf. Keller 1985).

It is interesting to compare the accuracy of the WKB prediction of the axial wavenumbers $\widetilde{k}$ based on the dispersion relation (3.13) with the well-known exact solution of system (3.1)–(3.3) for a uniform mean flow in a duct with hard walls. If M' is identically zero and $z_h = z_d = \infty$, the system (3.1)–(3.3) reduces to the boundary value problem for the Bessel equation

$$\frac{\mathrm{d}^2 P}{\mathrm{d}r^2} + \frac{1}{r}\frac{\mathrm{d}P}{\mathrm{d}r} + \left(\alpha^2 - \frac{m^2}{r^2}\right) P = 0, \quad \frac{\mathrm{d}P}{\mathrm{d}r} = 0 \quad \text{at} \quad r = s, 1,$$

and with the dispersion relation being

$$J'_m(\alpha s) Y'_m(\alpha) - Y'_m(\alpha s) J'_m(\alpha) = 0, \quad \alpha = \sqrt{(\omega - M\widetilde{k})^2 - \widetilde{k}^2},$$

where the primes stand for derivatives of the Bessel functions with respect to their arguments.

The results of a comparison between the WKB approximation (3.13) of the eigenvalues $\widetilde{k}$ and their exact counterparts based on the above formula are summarized in table 1, which shows the first five complex eigenvalues for $\widetilde{\omega} = 25$, $m = 15$, $s = 0.6$, $M = 0.5$. It can be seen from table 1 that the exact and the predicted values of the real parts of the axial wavenumbers $\widetilde{k}$ coincide. Apart from the first axial wavenumber $\widetilde{k}$ with the smallest absolute value, for which the relative error is 3.6%, the WKB prediction for the imaginary part of $\widetilde{k}$ is also very good, and the accuracy improves as $|\widetilde{k}|$ grows. This remarkable feature of the WKB approximation can be used to check the accuracy of numerical schemes for large $\widetilde{\omega}$, m, where the accuracy of the WKB approximation becomes even better whereas the accuracy of numerical schemes decreases owing to the stiffness of the problem.

3.1.2. *Narrow-duct approximation*

In general, the roots of equations (3.12) or (3.13) must be found numerically. One exception is the case of a narrow-duct approximation ($\Delta = 1 - s \to 0$) with linear, almost uniform mean flow $M = M_0 + M_1(r - s) + O(\Delta^2)$, and rotating phase planes given by $\omega t = m\vartheta + kx$, where $\tilde{\omega} \sim m \sim \tilde{k} \gg 1$. Then the duct width $\Delta = 1 - s \ll 1$ and we approximate

$$\tau(r) = \sqrt{q(s)}(r - s) + \frac{q'(s)}{\sqrt{q(s)}} \frac{(r - s)^2}{4} + O(\Delta^3), \quad s \leqslant r \leqslant 1,$$

since it was assumed that $q(r) \neq 0$. Making use of the expansion $q(r) = (\tilde{\omega} - \tilde{k}M)^2 - \tilde{k}^2 - m^2/r^2 + O(1)$ as $\tilde{k} \to \infty$ and taking $r = 1$, yields for the dispersion relation

$$q(s) = \left(\frac{\pi n}{\Delta}\right)^2 - \tfrac{1}{2}q'(s)\Delta + \cdots,$$

with solution $\tilde{k} = \tilde{k}_n$, where

$$k_n = \frac{-0.5\tilde{\omega}(M_h + M_d) \pm \sqrt{D}}{1 - M_h M_d}, \tag{3.14}$$

$$D = \tilde{\omega}^2 - (1 - M_h M_d)\left\{\left(\frac{m}{s}\right)^2\left(1 - \frac{\Delta}{s}\right) + \left(\frac{\pi n}{\Delta}\right)^2\right\} + O(\Delta^2).$$

Here and in what follows n is the same integral number as appears on the right of equation (3.13). This solution is perfectly analogous to the uniform mean flow solution which is recovered when M_h is set equal to M_d. The eigenvalues (3.14) are distributed symmetrically with respect to the real axis in the complex plane $\tilde{k}$, and as n goes to infinity with $\tilde{\omega}$ and m being fixed, $\tilde{k}$ approaches the vertical line $\tilde{k} = -0.5\tilde{\omega}(M_h + M_d)/(1 - M_h M_d)$.

Numerical analysis also confirms that in the high-frequency limit considered here the effect of mean flow shear on the acoustic part of the spectrum is moderate, provided regions with strong shear gradients are absent. However, quantitative differences between the predictions of the values of modal wavenumbers based on the uniform and the shear flow models may be perceptible. These are shown in figure 2, illustrating how the modal structure changes as the main flow changes from the uniform profile $M = 0.35$ to the linear and parabolic profiles given by

$$M(r) = \frac{M_h - M_d}{s - 1}(r - 1) + M_d, \; M(r) = (M_d - M_h)\left(\frac{r - 1}{s - 1} - 1\right)^2 + M_h, \tag{3.15}$$

respectively. Here $M_h = 0.5$, $M_h = 0.2$ and $s = 0.5$. Both profiles have a velocity maximum at the inner wall. It can be inferred from the figure that topologically all three patterns of axial wavenumber distributions are similar and feature the same number of cut-on modes. However, the actual values of the wavenumbers depend on the mean flow profile. The main differences are the deviation of the first several complex eigenvalues from the vertical direction and the leftward shift of the whole pattern for the parabolic profile, which is due to the increase of the average speed of the mean flow.

3.1.3. *Effects of lining*

According to the results recently reported by Rienstra (2003*b*) for the lined circular duct with uniform mean flow, the problem for a lined duct may be expected to

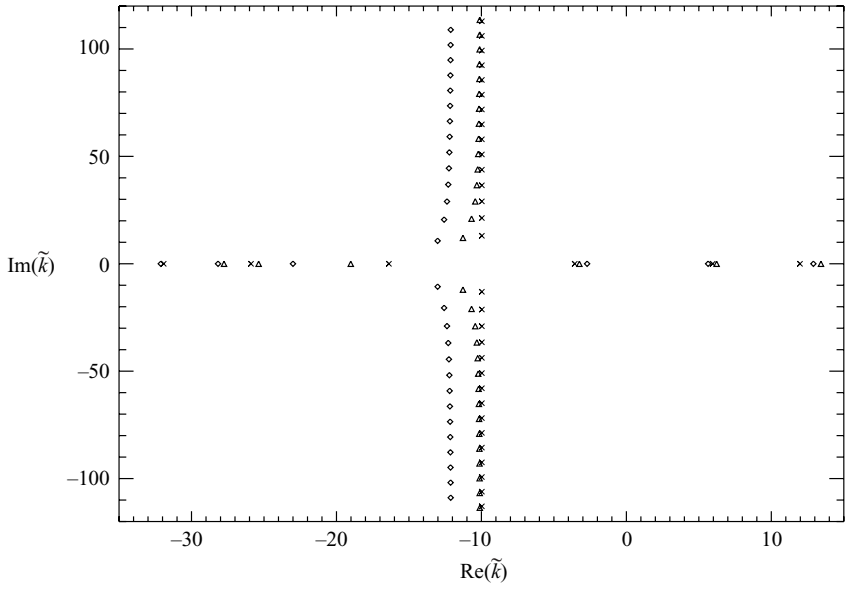

FIGURE 2. Effect of mean flow non-uniformity on the acoustic part of the axial wavenumber spectrum, $\widetilde{\omega}=25$, $m=15$, $s=h/d=0.5$. $\times$, uniform flow ($M=0.35$); $\triangle$, linear profile ($M_h=0.5$, $M_d=0.2$); $\diamond$, parabolic profile ($M_h=0.5$, $M_d=0.2$).

feature a much richer behaviour. Owing to the complicated character of the dispersion relation (3.12), a further simplifying assumption that the modes are well cut-off, i.e. $\widetilde{\omega} \approx |m| \ll |\widetilde{k}|$ as $\widetilde{k} \to \infty$, is needed to make this case analytically treatable.

It should be noted that although from the practical point of view the cut-on and close to cut-on modes are of the most importance for the propagation problem, knowledge of a large number of cut-off modes is sometimes needed in industrial applications. As already mentioned in the Introduction, one such example (which has triggered the present study) is the problem of spectral approximation of the perturbation pressure field created in the vicinity of an aero-engine fan in a ducted flow with shear. The benefit of the proposed asymptotic analysis is that it gives a rather accurate prediction of the topological structure of the spectrum in the complex wavenumber plane $\widetilde{k}$ for varying wall impedance even for the lowest cut-off mode numbers (as illustrated in figure 3*a* below). This is particularly important for lined walls with finite resistance, in which case the cut-on wavenumbers may move into the complex plane and become cut-off.

For simplicity let us assume that the inner wall is hard so that $\sigma_h=0$ and $\zeta=(1+\sigma_d)/(1-\sigma_d)$. Equation (3.12) then can be rewritten in the form

$$2\mathrm{i}\tau_d = -2\pi n\mathrm{i} + \ln\left(\frac{z_d+z_0}{z_d-z_0}\right), \quad \text{where} \quad z_0=\frac{(\widetilde{\omega}-\widetilde{k}M_d)^2}{\widetilde{\omega}\sqrt{q(1)}}, \tag{3.16}$$

and n is an integer. Note that for large $\widetilde{k}$ the logarithmic term in (3.16) is $O(1)$ when $z_0 \neq \pm z_d$ whereas $\tau_d=O(\widetilde{k})$. Hence to leading order, the solution to equation (3.16) is governed by the dispersion relation obtained above for the hard-wall boundary conditions $\tau_d \approx -\pi n$, where $|n|$ is large. The logarithmic term influences higher-order

terms. Expanding z_0 and τ_d in powers of $\widetilde{k}$

$$z_0 = -\mathrm{i}\zeta_1\widetilde{k} + \mathrm{i}\zeta_0 + O(\widetilde{k}^{-1}), \quad \tau_d = \mathrm{i}\kappa_1\widetilde{k} + \mathrm{i}\kappa_0 - \mathrm{i}\kappa_{-1}\widetilde{k}^{-1} + O(\widetilde{k}^{-2})$$

and substituting these formulae in (3.16) gives

$$\widetilde{k} + \frac{\kappa_0}{\kappa_1} - \frac{\kappa_{-1}}{\kappa_1}\widetilde{k}^{-1} + O(\widetilde{k}^{-2}) = \frac{\pi n\mathrm{i}}{\kappa_1} - \frac{1}{2\kappa_1}\ln\frac{z_d - \mathrm{i}(\zeta_1\widetilde{k} - \zeta_0 + O(\widetilde{k}^{-1}))}{z_d + \mathrm{i}(\zeta_1\widetilde{k} - \zeta_0 + O(\widetilde{k}^{-1}))}, \tag{3.17}$$

where

$$\zeta_1 = \frac{\widetilde{\omega}^{-1}M_d^2}{\sqrt{1-M_d^2}}, \quad \zeta_0 = \frac{(2-M_d^2)M_d}{(1-M_d^2)^{3/2}},$$

$$\kappa_1 = \int_s^1 \sqrt{1-M^2}\,\mathrm{d}r, \quad \kappa_0 = \int_s^1 \frac{\widetilde{\omega}M\,\mathrm{d}r}{\sqrt{1-M^2}},$$

$$\kappa_{-1} = \frac{1}{2}\int_s^1 \left\{\frac{\widetilde{\omega}^2}{1-M^2} - \frac{m^2}{r^2} - \frac{2M'^2}{M^2} + \frac{M'' + M'/r}{M} + \frac{1}{4r^2}\right\}\frac{\mathrm{d}r}{\sqrt{1-M^2}}.$$

Consider first the hard-wall limit $|z_d| \gg \zeta_1\pi n/\kappa_1 \gg 1$ with the real and imaginary parts of the impedance z_d being of the same order of magnitude. Since $|\widetilde{k}| \sim \pi n/\kappa_1$, the logarithmic term on the right-hand side of (3.17) can be further simplified, and the following solution for $\widetilde{k}$ can be obtained:

$$\widetilde{k} = \left\{\frac{\pi n\mathrm{i}}{\kappa_1} - \frac{\kappa_0}{\kappa_1} - \frac{\mathrm{i}\kappa_{-1}}{\pi n}\cdots\right\} - \frac{1}{z_d}\left(\frac{\zeta_1\pi n}{\kappa_1^2} + \cdots\right). \tag{3.18}$$

Here the curly brackets contain the expansion of the hard-wall solution in powers of n. The second term is the leading-order correction due to the lining.

Let R and X be the real and imaginary parts of the specific impedance z_d, and $\widetilde{k}_r$ and $\widetilde{k}_i$ the real and imaginary part of the axial wavenumber $\widetilde{k}$. Then elimination of X from (3.18) yields the following relationship between $\widetilde{k}_r$ and $\widetilde{k}_i$:

$$\left(\widetilde{k}_r + \frac{\kappa_0}{\kappa_1} + \frac{\zeta_1\pi n}{2R\kappa_1^2}\right)^2 + \left(\widetilde{k}_i - \frac{\pi n}{\kappa_1} + \frac{\kappa_{-1}}{\pi n}\right)^2 = \left(\frac{\zeta_1\pi n}{2R\kappa_1^2}\right)^2. \tag{3.19}$$

Expression (3.19) shows that when the real part R of the impedance z_d is fixed and its complex part X is allowed to vary, the eigenvalues whose index n is not too large (i.e. $|z_d| \gg \zeta_1\pi n/\kappa_1 \gg 1$) travel along the circle which surrounds the corresponding hard-wall eigenvalue

$$\widetilde{k}^0 = \widetilde{k}_r^0 + \mathrm{i}\widetilde{k}_i^0,$$

where

$$\widetilde{k}_r^0 = -\frac{\kappa_0}{\kappa_1} + \cdots, \quad \widetilde{k}_i^0 = \frac{\pi n}{\kappa_1} - \frac{\kappa_{-1}}{\pi n} + \cdots. \tag{3.20}$$

Its radius decreases with the resistance R and the frequency $\widetilde{\omega}$ and grows with the Mach number and with the index n. The centre of the circle is shifted to the left from the position of the hard-wall eigenvalue $\widetilde{k}^0$ by an amount equal to its radius for positive n, and to the right for negative n. The neighbouring circles are shifted with respect to each other in the vertical direction by $\pi/\kappa_1 + O(1/n^2)$ which depends mainly on the Mach number distribution and the hub-to-tip ratio s. This result gives a theoretical explanation for the appearance of circular trajectories in the complex plane of the axial wavenumber for sufficiently large but fixed resistance R and varying X which were obtained numerically in Rienstra (2003*b*) for a lined duct with constant

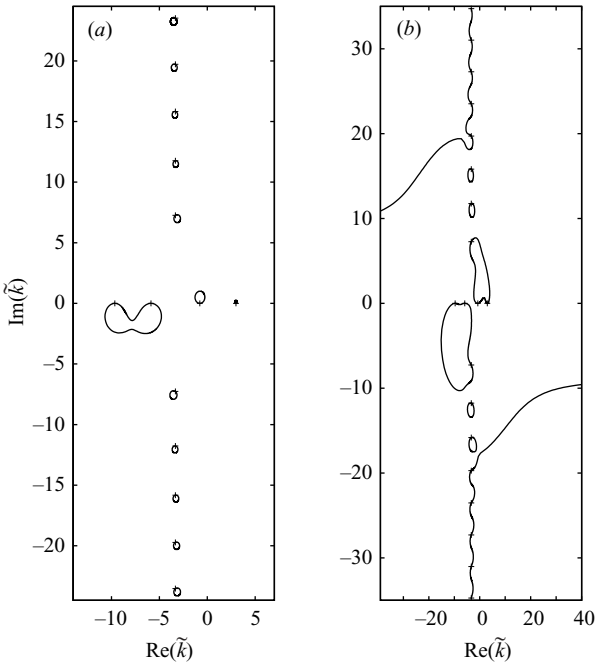

FIGURE 3. Trajectories of the axial wavenumber $\widetilde{k}$ for $\widetilde{\omega}=5$, $m=1$, $M=0.5$. (*a*) $z_d=2+\mathrm{i}X$, (*b*) $z_d=0.5+\mathrm{i}X$.

mean flow. This effect is also illustrated in figure 3(*a*) obtained by means of direct numerical solution of the Pridmore-Brown equation for a circular duct with $\widetilde{\omega}=5$, $m=1$, $z_d=2+\mathrm{i}X$ and the uniform mean flow profile $M=0.5$. Owing to the difference in the sign convention before the term $\mathrm{i}\omega t$ in Rienstra (2003*b*) and the present study, the direction of the horizontal shifts of the circles (3.19) is opposite.

It can be inferred from figure 3(*a*) that the real-valued wavenumbers which are cut-on in the hard-wall case move off the real axis and become cut-off for an impedance wall with finite resistance R. Like their strongly cut-off counterparts, these modes also follow circular trajectories, when the resistance R is large. This is the case with the two right-hand side cut-on modes shown in figure 3(*a*).

Consider now a more general situation when $|z_d|\sim\zeta_1\pi n/\kappa_1\gg 1$, in which case it follows from (3.17) that

$$\widetilde{k}=\widetilde{k}_r^0+\mathrm{i}\widetilde{k}_i^0-\frac{1}{2\kappa_1}\ln\left(\frac{z_d+\zeta_1\pi n/\kappa_1+\mathrm{i}(\zeta_1\kappa_0/\kappa_1-\zeta_0)}{z_d-\zeta_1\pi n/\kappa_1-\mathrm{i}(\zeta_1\kappa_0/\kappa_1+\zeta_0)}\right)+O(n^{-2}). \tag{3.21}$$

Note that expansion (3.18) can be obtained from (3.21) in the limit $|z_d|\gg\zeta_1\pi n/\kappa_1$.

For $|z_d|\sim\zeta_1\pi n/\kappa_1$ solution (3.21) breaks down in the vicinities of the points where

$$z_d=-\frac{\zeta_1\pi n}{\kappa_1}-\mathrm{i}\left(\frac{\zeta_1\kappa_0}{\kappa_1}-\zeta_0\right)\quad\text{or}\quad z_d=\frac{\zeta_1\pi n}{\kappa_1}+\mathrm{i}\left(\frac{\zeta_1\kappa_0}{\kappa_1}+\zeta_0\right). \tag{3.22}$$

If the value of the specific impedance z_d is sufficiently close to any of these points, the logarithmic term on the right-hand side of (3.17) becomes comparable with the first term $\pi n/\kappa_1$and the main-order solution is not governed by the hard-wall approximation any more. Thus, it must be assumed that z_d does not lie in the immediate vicinity of the points (3.22). The case when the logarithmic term on

the right-hand side of (3.17) dominates over $\pi n/\kappa_1$will be studied in what follows. However analytical treatment of the situation when these terms are of the same order of magnitude was difficult and will be tackled numerically elsewhere.

Taking the real and imaginary parts of (3.21) leads to the formulae

$$\widetilde{k}_r - \widetilde{k}_r^0 = -\frac{1}{4\kappa_1}\ln\left\{\frac{(R^2+(\zeta_0-X)^2-A^2-B^2)^2+4(BR+A(\zeta_0-X))^2}{[(R-A)^2+(B+\zeta_0-X)^2]^2}\right\}, \quad (3.23)$$

$$\tan\widetilde{\psi} = -\frac{2(BR+A(\zeta_0-X))}{R^2+(\zeta_0-X)^2-A^2-B^2}, \quad \widetilde{\psi} = 2\kappa_1\left(\widetilde{k}_i - \widetilde{k}_i^0\right). \quad (3.24)$$

Here $A=\zeta_1\pi n/\kappa_1$, $B=\zeta_1\kappa_0/\kappa_1$. Assume now that $|A|\sim|X|\gg R$. Relations (3.23), (3.24) then can be used to write $\widetilde{k}_r$ in terms of $\widetilde{k}_i$:

$$\zeta_0 - X \approx \frac{A}{\sin\widetilde{\psi}}(\cos\widetilde{\psi}\pm 1), \quad \widetilde{k}_r - \widetilde{k}_r^0 \approx \frac{1}{\kappa_1}\frac{B(\zeta_0-X)-RA}{(\zeta_0-X)^2+A^2}$$

and hence

$$\widetilde{k}_r - \widetilde{k}_r^0 = \frac{-R\cos(2\kappa_1(\widetilde{k}_i-\widetilde{k}_i^0))+B\sin\left(2\kappa_1\left(\widetilde{k}_i-\widetilde{k}_i^0\right)\right)-R}{2A\kappa_1} \quad \text{if } X/A>0, \quad (3.25)$$

$$\widetilde{k}_r - \widetilde{k}_r^0 = \frac{-R\cos(2\kappa_1(\widetilde{k}_i-\widetilde{k}_i^0))-B\sin\left(2\kappa_1\left(\widetilde{k}_i-\widetilde{k}_i^0\right)\right)+R}{2A\kappa_1} \quad \text{if } X/A<0. \quad (3.26)$$

Formulae (3.25), (3.26) show that when resistance R is small and kept fixed while reactance X varies, the eigenvalue $\widetilde{k}$ with a sufficiently large index n must move along the sinusoidal line. The zeros of this line coincide with the hard-wall eigenvalues $\widetilde{k}^0=\widetilde{k}_r^0+\mathrm{i}\widetilde{k}_i^0$. For instance, if for some $n>0$ (or $n<0$) the corresponding eigenvalue $\widetilde{k}^0(n)$ is taken as a starting point at $X=+\infty$ and then X is allowed to gradually vary until $X=-\infty$, then on moving along the line (3.25) (or (3.26), respectively) the eigenvalue value $\widetilde{k}$ will terminate at the point $\widetilde{k}^0(n+1)$ (or $\widetilde{k}^0(n-1)$, respectively) as illustrated in figure 3(*b*) which was obtained numerically. This behaviour can be also noticed directly from formula (3.21). Indeed, as the point z_d moves along the line parallel to the imaginary axis from the position $z_d=R+\mathrm{i}\infty$ to $z_d=R-\mathrm{i}\infty$ and passes singular points (3.22), but does not cross them, the imaginary part of the logarithm in (3.21) increases by -2π. As a result, the imaginary part of the eigenvalue $\widetilde{k}$ has an overall increment of π/κ_1. The amplitude of the sinusoidal lines (3.25), (3.26) decays as $1/n$ as $n\to\infty$. Note that the results obtained are exactly in line with the related numerical findings presented in figure 7 of Rienstra (2003*b*).

3.1.4. *Surface modes*

Only small corrections to the hard-wall solutions have been considered so far. The first such solution was based on the assumption that $R\gg\zeta_1\pi n/\kappa_1\gg 1$ and corresponded to the emergence of circular trajectories in the plane $\widetilde{k}$. The second solution was obtained in the limit $\zeta_1\pi n/\kappa_1\gg R$ and resulted in sinusoidal eigenvalue contours (3.25), (3.26). Consider now the case when z_0 is close to either of the points $\pm z_d$ and the logarithmic term in (3.16) is large. To construct relevant solutions, we assume that $|X|$ is large, the wall Mach number M_d does not vanish and $\widetilde{k}\to\infty$. Dispersion relation (3.16) can then be rewritten in the form

$$\exp[-2\kappa_1(\widetilde{k}+\kappa_0+O(\widetilde{k}^{-1}))] = \frac{z_d-\mathrm{i}(\zeta_1\widetilde{k}-\zeta_0+O(\widetilde{k}^{-1}))}{z_d+\mathrm{i}(\zeta_1\widetilde{k}-\zeta_0+O(\widetilde{k}^{-1}))}. \quad (3.27)$$

Its leading-order solutions are

$$\widetilde{k} = -\mathrm{i}z_d/\zeta_1 + \cdots \quad \text{if } X \to -\infty \quad \text{and } \widetilde{k} = \mathrm{i}z_d/\zeta_1 + \cdots \text{ if } X \to +\infty. \tag{3.28}$$

These solutions are analogous to the high-frequency surface-wave modes studied in Rienstra (2003*b*) in the context of a circular duct in a uniform flow. It is interesting to observe that although they do not have a hard-wall counterpart, the eigenvalues (3.28) follow from the same dispersion relation as the rest of the acoustic modes. When the wall Mach number $M_d = 0$, although there should be acoustic surface waves, formulae (3.28) do not apply. This situation should be tackled numerically.

3.2. *Turning points*

Assume that the function $q(r)$ from (3.5)–(3.7) has a simple zero at a point $r = r_*$, $s < r_* < 1$. Then, as is known, ordinarily the WKB procedure is not valid near r_* and should be modified so as to retain the structure of the function $q(r)$ in the main part of the operator on the right-hand side of (3.5). This can be accomplished by taking

$$\tau(r) = \left\{ \frac{3}{2} \int_{r_*}^{r} \sqrt{q(\xi)}\, \mathrm{d}\xi \right\}^{2/3}.$$

Then assuming that $m \sim \widetilde{\omega} \sim \widetilde{k}$ as $\widetilde{k} \to \infty$ and also (3.9), in order to keep the impedance term in the boundary condition, the problem (3.5)–(3.7) becomes

$$\frac{\mathrm{d}^2 w}{\mathrm{d}\tau^2} + \tau w = 0, \quad \frac{\mathrm{d}w}{\mathrm{d}\tau} + \mathrm{i}\sigma_h w = 0 \quad \text{at } \tau = \tau_h, \quad \frac{\mathrm{d}w}{\mathrm{d}\tau} - \mathrm{i}\sigma_d w = 0 \quad \text{at } \tau = \tau_d, \tag{3.29}$$

where $\tau_h = \tau(s)$, $\tau_d = \tau(1)$, and σ_h and σ_d are given by (3.11). System (3.29) has solution $w(\tau) = A\,\mathrm{Ai}(-\tau) + B\,\mathrm{Bi}(-\tau)$, where Ai and Bi are Airy functions, which is not identically zero if

$$I(\widetilde{k}) = \begin{vmatrix} \mathrm{Ai}'(-\tau_d) + \mathrm{i}\sigma_d\,\mathrm{Ai}(-\tau_d) & \mathrm{Bi}'(-\tau_d) + \mathrm{i}\sigma_d\,\mathrm{Bi}(-\tau_d) \\ \mathrm{Ai}'(-\tau_h) - \mathrm{i}\sigma_h\,\mathrm{Ai}(-\tau_h) & \mathrm{Bi}'(-\tau_h) - \mathrm{i}\sigma_h\,\mathrm{Bi}(-\tau_h) \end{vmatrix} = 0. \tag{3.30}$$

To main order in $\widetilde{k}$ the position of the turning point is given by $(\widetilde{\omega} - \widetilde{k}M(r_*))^2 - \widetilde{k}^2 - m^2/r_*^2 = 0$, or equivalently,

$$\widetilde{k} = \frac{-\widetilde{\omega}M(r_*) \pm \sqrt{\widetilde{\omega}^2 - (1 - M^2(r_*))m^2/r_*^2}}{1 - M(r_*)^2}, \tag{3.31}$$

where $\widetilde{k}$ and r_* are to be found. Since $r_* > s > 0$, we assume in what follows that the non-dimensional frequency $\widetilde{\omega}$ is large enough for the square root in (3.31) to be real. This is also the most important situation practically. In this case the axial wavenumber $\widetilde{k}$ and the function $q(r)$ are also real and, hence, either $q'(r_*) > 0$ or $q'(r_*) < 0$.

Consider first the inequality $q'(r_*) > 0$. Then as $\widetilde{k} \to \infty$

$$\tau_h = \left\{ -\frac{3}{2}\mathrm{i} \int_{s}^{r_*} \sqrt{|q(\xi)|}\, \mathrm{d}\xi \right\}^{2/3} \to -\infty, \quad \tau_d = \left\{ \frac{3}{2} \int_{r_*}^{1} \sqrt{q(\xi)}\, \mathrm{d}\xi \right\}^{2/3} \to +\infty$$

and the dispersion relation (3.30) yields

$$\cos\left(\zeta_d + \tfrac{1}{4}\pi\right) - \mathrm{i}\sigma_d \tau_d^{-1/2} \sin\left(\zeta_d + \tfrac{1}{4}\pi\right) + \cdots = 0, \tag{3.32}$$

where $\zeta_d = \int_{r_*}^{1} \sqrt{q(\xi)}\,\mathrm{d}\xi$. Together with (3.31), formula (3.32) defines the positions of the turning points r_*. The corresponding modal solution has the following asymptotic structure (as $\widetilde{k} \to \infty$):

$$w = \left\{\sin\left(\zeta_d + \tfrac{1}{4}\pi\right) + \mathrm{i}\sigma_d \tau_d^{-1/2} \cos\left(\zeta_d + \tfrac{1}{4}\pi\right) + \cdots\right\} \mathrm{Ai}(-\tau) + \left\{\cos\left(\zeta_d + \tfrac{1}{4}\pi\right) - \mathrm{i}\sigma_d \tau_d^{-1/2} \sin\left(\zeta_d + \tfrac{1}{4}\pi\right) + \cdots\right\} \mathrm{Bi}(-\tau).$$

If there exists r_* such that the dispersion relation (3.32) is satisfied, then the coefficient before the function $\mathrm{Bi}(-\tau)$ is identically zero. In this case the eigenfunction w decays exponentially in the interval $s < r < r_*$, where $q(r) < 0$, and oscillates in the interval $r_* < r < 1$, where $q(r) > 0$. As a result, it is the boundary condition at the outer wall, where $q(r) > 0$, that has the major influence on the existence and the character of the roots r_* of the dispersion relation, whereas the character of the boundary condition in the quiet region $s < r < r_*$, where $q(r) < 0$, is relatively unimportant.

Substituting σ_d from (3.11), $z_d = R + \mathrm{i}X$, using the identity $\tau' \tau^{1/2} = \sqrt{q(r)}$ and taking the real and imaginary part of (3.32) we obtain the system

$$\left.\begin{aligned} \cos\left(\zeta_d + \tfrac{1}{4}\pi\right) - \frac{X}{R^2 + X^2} \frac{(\widetilde{\omega} - \widetilde{k} M_d)^2}{\widetilde{\omega}\sqrt{q(1)}} \sin\left(\zeta_d + \tfrac{1}{4}\pi\right) = 0, \\ \frac{R}{R^2 + X^2} \sin\left(\zeta_d + \tfrac{1}{4}\pi\right) = 0. \end{aligned}\right\} \tag{3.33}$$

If $z_d = \infty$, (3.33) reduces to the hard-wall case considered in Cooper & Peake (2005) (see their formula (103) with $\psi = 0$)

$$\int_{r_*}^{1} \sqrt{q(r)}\,\mathrm{d}r = \pi\left(n + \tfrac{1}{4}\right), \quad n = 0, 1, 2, 3 \ldots. \tag{3.34}$$

It follows from (3.33) that the problem with the lined outer wall does not admit real turning points, apart from the very special case of $R = 0$ when system (3.33) reduces to

$$\sqrt{(\widetilde{\omega} - \widetilde{k} M_d)^2 - \widetilde{k}^2 - m^2} = \frac{(\widetilde{\omega} - \widetilde{k} M_d)^2}{\widetilde{\omega} X} \tan\left(\zeta_d + \tfrac{1}{4}\pi\right). \tag{3.35}$$

Consider now the inequality $q'(r_*) < 0$. Then as $\widetilde{k} \to \infty$

$$\tau_h = \left\{\frac{3}{2}\int_{s}^{r_*} \sqrt{q(\xi)}\,\mathrm{d}\xi\right\}^{2/3} \to +\infty, \quad \tau_d = \left\{\frac{3}{2}\int_{r_*}^{1} \sqrt{|q(\xi)|}\,\mathrm{d}\xi\right\}^{2/3} \to -\infty$$

and the dispersion relation (3.30) yields

$$\cos\left(\zeta_h + \tfrac{1}{4}\pi\right) + \mathrm{i}\sigma_h \tau_h^{-1/2} \sin\left(\zeta_h + \tfrac{1}{4}\pi\right) + \cdots = 0, \tag{3.36}$$

where $\zeta_h = -\int_{s}^{r_*} \sqrt{q(\xi)}\,\mathrm{d}\xi$. The solution w now has the following structure (as $\widetilde{k} \to \infty$):

$$w = \left\{\sin\left(\zeta_h + \tfrac{1}{4}\pi\right) - \mathrm{i}\sigma_h \tau_h^{-1/2} \cos\left(\zeta_h + \tfrac{1}{4}\pi\right) + \cdots\right\} \mathrm{Ai}(-\tau) - \left\{\cos\left(\zeta_h + \tfrac{1}{4}\pi\right) + \mathrm{i}\sigma_h \tau_h^{-1/2} \sin\left(\zeta_h + \tfrac{1}{4}\pi\right) + \cdots\right\} \mathrm{Bi}(-\tau).$$

Again, the solution oscillates in the region, where $q(r) > 0$ (i.e. $s < r < r_*$), and exponentially decays in the region, where $q(r) < 0$ (i.e. $r_* < r < 1$), provided that the dispersion relation (3.36) holds at the turning point r_*. As a result, now the boundary condition on the inner wall $r = s$ is of major importance, whereas the outer wall lies in the quiet zone. The analysis of equation (3.36) is identical to the analysis

WKB tp $\widetilde{k}_{tp}$	Exact $\widetilde{k}$	Relative error % $\lvert\widetilde{k}_{tp}-\widetilde{k}\rvert/\lvert\widetilde{k}-\widetilde{k}_d\rvert$
−43.36	−43.59	1.38
−38.00	−38.36	2.16
−31.12	−32.08	6.23
−2.210	−1.251	6.22
4.564	5.028	2.14
10.45	10.26	0.72

TABLE 2. Turning-point analysis versus exact solution.

of (3.32), with the main result being that no turning points are possible if the real part of the wall impedance z_h is non-zero.

Overall we see that if the wall, where the function $q(r)$ has a positive value, is treated with a lining material with finite resistance the dispersion relation (3.30) cannot be satisfied for any r_* lying inside the flow region. As a result, there exist no solutions with real turning points and cut-on wavenumbers $\widetilde{k}$ defined by formula (3.31) in this case. This is in line with the numerical results presented in figure 3(*a*), which show that all cut-on modes are shifted off the real axis when the resistance R is taken to be non-zero on an appropriately chosen wall.

Contrary to this, the properties of the lining material on the wall, where the function $q(r)$ is negative, do not have significant effect on the roots of the dispersion relation. In this case the wall is located inside the quiet region and to leading order the dispersion relation is unaffected by this wall's impedance. This is the wall $r=s$ in the case of the dispersion relation (3.30) and the wall $r=1$ in the case of the dispersion relation (3.31). For example, if $q(r=s)<0$ and $q(r=1)>0$, the wall $r=s$ is soft and the wall $r=1$ is hard, then to leading order the turning points are given by equation (3.34) or, equivalently $\cos(\zeta_d+\frac{1}{4}\pi)=0$. If $q(r=s)>0$ and $q(r=1)<0$, the wall $r=s$ is hard and the wall $r=1$ is soft, then the turning points are given by the equation $\cos(\zeta_h+\frac{1}{4}\pi)=0$.

As with the ordinary WKB approximation, it is useful to check the accuracy of the approximate formula (3.34) against the related exact uniform flow solutions with $\widetilde{k}$ real. The results of the comparison are shown in table 2 for the same values of governing parameters as in table 1: $\widetilde{\omega}=25$, $m=15$, $s=0.6$, $M=0.5$, $z_d=\infty$. In computation of the relative error in table 2 an adjustment for the Doppler shift $\widetilde{k}_d$ in $\widetilde{k}$ equal to -16.67 was made. It can be seen from table 2 that the accuracy is reasonably good, although it decreases significantly when the turning point is located very close to the duct wall. This situation is illustrated in the fourth row of the table. Here the turning point actually lies slightly inside the hub, i.e. $r_{tp}=0.589<s=0.6$ and the related eigenvalue must be taken from the ordinary WKB analysis. However, the turning-point prediction was found to be in perceptibly better agreement with the exact solution.

3.3. *Hydrodynamic spectrum*

The analysis carried out in the previous sections assumed that $\widetilde{\omega}-\widetilde{k}M(r)$ did not vanish, so that the coefficients of the governing equation remained smooth in r. This section aims to study the properties of the eigensolutions of system (3.1)–(3.3) when $\widetilde{\omega}-\widetilde{k}M(r)=0$ at some point $r=\widetilde{r}$, $s\leqslant\widetilde{r}\leqslant 1$. In this case the coefficient before the

first derivative in equation (3.1) goes to infinity and the function $q(r)$ defined by (3.8) develops a singularity near $\tilde{r}$. The Pridmore-Brown equation has a regular singular point at $r=\tilde{r}$ and its two linearly independent solutions in the vicinity of this point are (see, for example, Korn & Korn 1968)

$$p_1(r) = (r-\tilde{r})^3 \sum_{n=0}^{\infty} a_n (r-\tilde{r})^n,$$

$$p_2(r) = -\frac{b_0}{3a_0}\left(\left(\frac{M''(\tilde{r})}{M'(\tilde{r})} - \frac{1}{\tilde{r}}\right)\left(\tilde{k}^2 + \frac{m^2}{\tilde{r}^2}\right) + \frac{2m^2}{\tilde{r}^3}\right) p_1(r)\ln(r-\tilde{r}) + \sum_{n=0}^{\infty} b_n (r-\tilde{r})^n,$$

where $a_0 \neq 0$ and $b_0 \neq 0$ are arbitrary numbers and the coefficients a_n, b_n are fixed functions of a_0 and b_0, respectively. The details of the procedure used to obtain solutions of this type are also documented in Lees & Lin (1946). General solution to equation (3.1) is regular near the critical point $\tilde{r}$ provided the following smoothness condition is satisfied:

$$\left(\frac{M''(\tilde{r})}{M'(\tilde{r})} - \frac{1}{\tilde{r}}\right)\left(\tilde{k}^2 + \frac{m^2}{\tilde{r}^2}\right) + \frac{2m^2}{\tilde{r}^3} = 0.$$

If otherwise, the general solution is singular and the problem (3.1)–(3.3) may have a critical layer near the point $\tilde{r}$ with the axial velocity amplitude $U(r) = O(\ln(r-\tilde{r}))$ as r goes to $\tilde{r}$. If $\tilde{k}$ and m are both assumed large, while the derivatives of the Mach number remain $O(1)$ at $\tilde{r}$, further analytical advance is possible. This case is studied in the next section, and the main result obtained is that in the short-wavelength limit there cannot exist more than two hydrodynamic modes which are smooth for $s < r < 1$. They correspond to the critical point $\tilde{r}$ lying on either of the duct walls. However, apart from these two modes, there also exists a continuum of hydrodynamic modes with a singularity lying inside the interval $s < r < 1$.

3.3.1. *Narrow duct*

Hydrodynamic modes with the critical point on the duct wall

The ordinary WKB solution constructed in the previous sections becomes invalid at the point $\tilde{r}$, although it still gives the correct outer limit of the solution for large $\tilde{k}$ as $r \to \tilde{r}$. In order to clarify the structure of the inner solution near $\tilde{r}$, first we consider a model problem for a narrow duct. The procedure of matching of the outer WKB solution with the corresponding leading-order inner solution which does not assume that the duct is narrow is described in the second part of this section. This procedure can be extended to a more general equation (2.24), in order to include the effects of the mean-flow swirl. It should be noted, however, that equation (2.24) has a stronger singularity than equation (3.1) and the results of this section are not directly applicable to the swirling flow. For simplicity in this section only the case of hard walls is considered.

Let $\Delta_+ = 1-\tilde{r}$, $\Delta_- = \tilde{r}-s$, $\Delta = 1-s$, where $0 < s \leqslant \tilde{r} \leqslant 1$, and assume that $\Delta \ll 1$. Introduce new independent variable $\eta = (r-\tilde{r})/\Delta$. Note that $\eta = O(1)$, since $-\Delta_-/\Delta \leqslant \eta \leqslant \Delta_+/\Delta$. Then

$$r^{-1} = \tilde{r}^{-1} + O(\Delta), \quad \tilde{\omega} - \tilde{k}M(r) = -\Delta\tilde{k}(M'(\tilde{r})\eta + O(\Delta)), \quad M(r) = M'(\tilde{r}) + O(\Delta).$$

We seek a solution of equation (3.1) in the form of the following expansion in Δ:

$$P = P_0(\eta) + \Delta P_1(\eta) + o(\Delta).$$

To leading order in Δ equation (3.1) becomes

$$\frac{\mathrm{d}^2 P_0}{\mathrm{d}\eta^2} - \frac{2}{\eta}\frac{\mathrm{d}P_0}{\mathrm{d}\eta} - \nu^2 P_0 = 0, \quad \frac{\mathrm{d}P_0}{\mathrm{d}\eta}\left(\eta = -\frac{\Delta_-}{\Delta}\right) = \frac{\mathrm{d}P_0}{\mathrm{d}\eta}\left(\eta = \frac{\Delta_+}{\Delta}\right) = 0. \tag{3.37}$$

Here we assume that $\nu^2 = \Delta^2(\widetilde{k}^2 + m^2/\widetilde{r}^2) = O(1)$. The first equation of system (3.37) has general solution

$$P_0 = c_+(1 - \nu\eta)\exp(\nu\eta) + c_-(1 + \nu\eta)\exp(-\nu\eta), \tag{3.38}$$

with $c_-, c_+ =$ constant. Substitution of (3.38) into the boundary conditions leads to the following system for c_- and c_+:

$$\frac{\mathrm{d}P_0}{\mathrm{d}\eta}\left(\eta = -\frac{\Delta_-}{\Delta}\right) = \nu^2\frac{\Delta_-}{\Delta}\left(c_+\exp\left(-\nu\frac{\Delta_-}{\Delta}\right) + c_-\exp\left(\nu\frac{\Delta_-}{\Delta}\right)\right) = 0,$$
$$\frac{\mathrm{d}P_0}{\mathrm{d}\eta}\left(\eta = \frac{\Delta_+}{\Delta}\right) = -\nu^2\frac{\Delta_+}{\Delta}\left(c_+\exp\left(\nu\frac{\Delta_+}{\Delta}\right) + c_-\exp\left(-\nu\frac{\Delta_+}{\Delta}\right)\right) = 0.$$

This system does not permit non-zero solutions for real $\widetilde{k}$ unless either $\Delta_+ = 0$ or $\Delta_- = 0$. Each of these cases leads to the eigensolution

$$P_0 = (1 + \nu\eta)\exp(-\nu(\eta - 1)) - (1 - \nu\eta)\exp(\nu(\eta - 1)), \tag{3.39}$$

where $\eta = (r-1)/\Delta$, $\nu = \Delta\sqrt{\widetilde{k}^2 + m^2}$, $\widetilde{k} = \widetilde{\omega}/M_d$, $M_d \neq 0$ for $\widetilde{r} = 1$ and $\eta = (r-s)/\Delta$, $\nu = \Delta\sqrt{\widetilde{k}^2 + m^2/s^2}$, $\widetilde{k} = \widetilde{\omega}/M_h$, $M_h \neq 0$ for $\widetilde{r} = s$. Note that in the special case when $M_d = M_h$, $\widetilde{k}$ is the eigenvalue of multiplicity two, as discussed in the Introduction.

It is interesting to observe that the main-order solution (3.39) is free of the logarithmic singularity obtained in the previous section for the function $p_2(r)$. This is not a discrepancy, however, since this singularity is fully recovered in the next-order term of the solution. Indeed, the next-order term $P_1(\eta)$ satisfies the following inhomogeneous boundary-value problem:

$$\frac{\mathrm{d}^2 P_1}{\mathrm{d}\eta^2} - \frac{2}{\eta}\frac{\mathrm{d}P_1}{\mathrm{d}\eta} - \nu^2 P_1 = -\left(b\frac{\mathrm{d}P_0}{\mathrm{d}\eta} + c\eta P_0\right), \quad \frac{\mathrm{d}P_1}{\mathrm{d}\eta}\left(-\frac{\Delta_-}{\Delta}\right) = \frac{\mathrm{d}P_1}{\mathrm{d}\eta}\left(\frac{\Delta_+}{\Delta}\right) = 0, \tag{3.40}$$

where

$$b = \frac{1}{\widetilde{r}} - \frac{M''(\widetilde{r})}{M'(\widetilde{r})} \quad \text{and} \quad c = \frac{2m^2}{\widetilde{r}^3}\Delta^2.$$

Here both b and c are assumed $O(1)$.

Consider, for definiteness, the case when the critical point lies on the inner wall $\eta = 0$, i.e. $\widetilde{r} = s$. The case when $\widetilde{r} = 1$ can be treated similarly. It can be shown after some simple but tedious algebra that the solution to equation (3.40) has the following form:

$$P_1 = C_+(\eta)p_+(\eta) + C_-(\eta)p_-(\eta),$$

where $p_+(\eta) = (\nu\eta - 1)\exp(\nu(\eta - 1))$, $p_-(\eta) = (\nu\eta + 1)\exp(-\nu(\eta - 1))$ are two linearly independent solution of the related homogeneous equation, and

$$C_\pm(\eta) = \pm\frac{c - b\nu^2}{2\nu^3}\int_0^\eta [1 - \exp(\mp 2\nu(\xi - 1))]\xi^{-1}\,\mathrm{d}\xi - \frac{1}{2}b(\eta - 1) \mp \frac{c}{4\nu}(\eta^2 - 1)$$
$$\pm\left(\frac{5c}{8\nu^3} - \frac{b}{4\nu}\right)[\exp(\mp 2\nu(\eta - 1)) - 1] + \frac{c}{4\nu^2}[\eta\exp(\mp 2\nu(\eta - 1)) - 1].$$

Any eigensolution proportional to $P_0(\eta)$) can, of course, be added to the solution P_1. It is easily seen from the expressions obtained that the most singular term of the solution P_1 as η goes to zero is

$$P_1 = \frac{1}{3}\left(\left(\frac{M''(\tilde{r})}{M'(\tilde{r})} - \frac{1}{\tilde{r}}\right)\left(\tilde{k}^2 + \frac{m^2}{\tilde{r}^2}\right) + \frac{2m^2}{\tilde{r}^3}\right)\Delta^2\eta^3 \ln\eta + \cdots.$$

Hence, we see that although the main-order solution is smooth, the singularity is recovered in the next-order term. As a result, the asymptotic solution obtained develops a logarithmic singularity near the critical point $r = \tilde{r}$ which lies on the wall of the duct in the short-wavenumber limit. It should be noted that here we have explicitly assumed that $\tilde{k}$ and m are of order Δ^{-1} or larger. This assumption is essential, since the expansion of the function P into a power series in Δ loses its asymptotic character if ν goes to zero, i.e. $\tilde{k}$ and $m \ll \Delta^{-1}$. When $\tilde{k}$ and m are not large, at least in principle, the problem can be expected to possess hydrodynamic eigensolutions if the smoothness condition of the previous section holds at the point $\tilde{r}$.

Singular hydrodynamic modes with the critical point lying strictly inside the duct

Apart from the two smooth eigensolutions described in the previous subsection, the leading-order problem (3.37) admits a continuous spectrum of solutions which have continuous derivatives up to the second order inclusive, but have a jump in the third derivative. These eigensolutions can be constructed as follows.

Consider the following two solutions of the differential equation (3.37):

$$P_0^-(\eta) = -\frac{\Delta}{\nu\Delta_-}\{(1-\nu\eta)\exp[\nu(\eta+\Delta_-/\Delta)] - (1+\nu\eta)\exp[-\nu(\eta+\Delta_-/\Delta)]\}$$

and

$$P_0^+(\eta) = \frac{\Delta}{\nu\Delta_+}\{(1-\nu\eta)\exp[\nu(\eta-\Delta_+/\Delta)] - (1+\nu\eta)\exp[-\nu(\eta-\Delta_+/\Delta)]\}.$$

It can be easily verified that

$$\frac{\mathrm{d}P_0^-}{\mathrm{d}\eta}\left(\eta = -\frac{\Delta_-}{\Delta}\right) = 0 \quad \text{and} \quad \frac{\mathrm{d}P_0^+}{\mathrm{d}\eta}\left(\eta = \frac{\Delta_+}{\Delta}\right) = 0,$$

so that the function

$$\psi = \begin{cases} P_0^+(0)P_0^-(\eta) & \text{if} \quad -\Delta_-/\Delta \leqslant \eta < 0, \\ P_0^-(0)P_0^+(\eta) & \text{if} \quad 0 < \eta \leqslant \Delta_+/\Delta, \end{cases}$$

satisfies the boundary conditions of the problem (3.37), has two continuous derivatives in η and also satisfies the differential equation of the problem (3.37) with the value of the spectral parameter $\tilde{k} = \tilde{\omega}/M(\tilde{r})$, where $s < \tilde{r} < 1$ is an arbitrary position of the critical point. However, the third derivative of the eigenfunction $\psi(\eta)$ is discontinuous at the point $\eta = 0$ which corresponds to the critical point $r = \tilde{r}$ in terms of the original radial coordinate.

We note in passing, that a higher-order analysis similar to the analysis in the previous section shows the emergence of the logarithmic term in the next-order approximation of the singular hydrodynamic modes considered here.

Although singular, these eigenmodes are of substantial practical importance. Indeed, consider the Green's function $G(\eta, \eta_0)$ for the system (3.37), i.e. the function $G(\eta, \eta_0)$

which satisfies the problem

$$\frac{\mathrm{d}^2G}{\mathrm{d}\eta^2}-\frac{2}{\eta}\frac{\mathrm{d}G}{\mathrm{d}\eta}-\nu^2G=\delta(\eta-\eta_0),\quad \frac{\mathrm{d}G}{\mathrm{d}\eta}(\eta=-\Delta_-/\Delta)=\frac{\mathrm{d}G}{\mathrm{d}\eta}(\eta=\Delta_+/\Delta)=0,$$

where $\delta(\eta)$ is the Dirac delta function and η_0 is the position of the source point, $-\Delta_-/\Delta<\eta_0<\Delta_+/\Delta$. It is easy to verify by direct calculation that

$$G(\eta,\eta_0)=\frac{1}{W(\eta_0)}\begin{cases}P_0^+(\eta_0)P_0^-(\eta) & \text{if}\quad -\Delta_-/\Delta\leqslant\eta<\eta_0,\\ P_0^-(\eta_0)P_0^+(\eta) & \text{if}\quad \eta_0<\eta\leqslant\Delta_+/\Delta.\end{cases}$$

where

$$W(\eta_0)=-\frac{2\Delta\nu\eta_0^2}{\Delta_-\Delta_+}(\mathrm{e}^{\nu}-\mathrm{e}^{-\nu}).$$

In can be seen from the last expression that the amplitude of the Green's function goes to infinity as the position of the source η_0 approaches the critical point $\eta=0$. In this case the expression to the right of the curly brackets in the formula for the Green's function is identically equal to the eigenfunction $\psi(\eta)$. This observation shows that the impulsive forcing on the right-hand side of the equation for $G(\eta,\eta_0)$ is in resonance with the system, due to the existence of the eigensolution $\psi(\eta)$, $\widetilde{k}=\widetilde{\omega}/M(\widetilde{r})$. As is known, this situation can be remedied by consideration of the generalized Green's function. The details of this approach can be found for instance in Smirnov (1981).

3.3.2. *A note on the general case of the Pridmore-Brown equation*

In this section our aim is to briefly outline the way in which the results of the previous section can be extended to the case of ducts that are not narrow.

For large $\widetilde{k}$ and away from the point $r=\widetilde{r}$ the WKB solution to the Pridmore-Brown equation (3.1) which satisfies the hard-wall boundary conditions is

$$P=\frac{\widetilde{\omega}-\widetilde{k}M}{\sqrt{r}}\frac{\cos(\tau)}{(\tau')^{1/2}}+\cdots,\quad \tau(r)=\int_a^r\sqrt{q(\xi)}\,\mathrm{d}\xi,\tag{3.41}$$

where $a=s>0$ if $s\leqslant r<\widetilde{r}$ and $a=1$ if $\widetilde{r}<r\leqslant 1$. If r is kept fixed and such that $r\neq\widetilde{r}$ and $\widetilde{k}\to\infty$ the function $q(r)$ previously defined by (3.8) becomes, to leading order,

$$q(r)=q_0(r),\quad \text{where}\quad q_0(r)=(\widetilde{\omega}-\widetilde{k}M)^2-\widetilde{k}^2-m^2/r^2,\tag{3.42}$$

since for the most singular term in (3.8) the estimate

$$\frac{2\widetilde{k}^2(M'(r))^2}{(\widetilde{\omega}-\widetilde{k}M(r))^2}=\frac{2(M'(r))^2}{(M(\widetilde{r})-M(r))^2}\leqslant\frac{\text{const}}{(\widetilde{r}-r)^2}\ll\widetilde{k}^2\tag{3.43}$$

holds provided $|\widetilde{r}-r|\gg 1/\widetilde{k}$ and $M'(r)$ is bounded for $s\leqslant r\leqslant 1$. In order to obtain outer asymptotic expansion of the solution near the point $\widetilde{r}$, substitute (3.42) in (3.41) and take the limit $r\to\widetilde{r}\pm$. This gives

$$P=-\frac{\widetilde{k}M'(\widetilde{r})(r-\widetilde{r})}{2\sqrt{\widetilde{r}\mu\mathrm{i}}}\left(\mathrm{e}^{-I_--\mu(r-\widetilde{r})}+\mathrm{e}^{I_-+\mu(r-\widetilde{r})}\right)+\cdots\quad\text{as}\quad r\to\widetilde{r}-,\tag{3.44}$$

$$P=-\frac{\widetilde{k}M'(\widetilde{r})(r-\widetilde{r})}{2\sqrt{\widetilde{r}\mu\mathrm{i}}}\left(\mathrm{e}^{-I_+-\mu(r-\widetilde{r})}+\mathrm{e}^{I_++\mu(r-\widetilde{r})}\right)+\cdots\quad\text{as}\quad r\to\widetilde{r}+,\tag{3.45}$$

where

$$I_- = \int_s^{\tilde{r}} \sqrt{-q_0(r)}\,\mathrm{d}r, \quad I_+ = \int_1^{\tilde{r}} \sqrt{-q_0(r)}\,\mathrm{d}r, \quad \mu = \sqrt{\tilde{k}^2 + m^2/\tilde{r}^2}.$$

Owing to the singularity (3.43), formulae (3.44), (3.45) are invalid in the region where $|\tilde{r}-r| \sim 1/\tilde{k}$, since in this region the singularity becomes comparable with the leading-order term $-\tilde{k}^2 - m^2/r^2$ in the expansion of $q(r)$. Prompted by the solution (3.39) of the model problem, introduce local coordinate $\xi = \mu(r-\tilde{r})$ which is centred on the singular point $\tilde{r}$ and is $O(1)$ in the region where $|\tilde{r}-r| \sim 1/\tilde{k}$. Then, to leading order, the Pridmore-Brown equation becomes

$$\frac{\mathrm{d}^2 P}{\mathrm{d}\xi^2} - \frac{2}{\xi}\frac{\mathrm{d}P}{\mathrm{d}\xi} - P = 0. \tag{3.46}$$

It must be supplemented with the conditions of matching with the main-order solution (3.44), (3.45) obtained in the outer region, i.e.

$$P(\xi \to \pm\infty) \to A\xi\left(\mathrm{e}^{-(I_\pm+\xi)} + \mathrm{e}^{(I_\pm+\xi)}\right) + \cdots, \quad A = -\frac{\tilde{k}M'(\tilde{r})}{2\sqrt{\tilde{r}}\mu^3 i}. \tag{3.47}$$

Equation (3.46) has general solution

$$P = c_+(1-\xi)\exp(\xi) + c_-(1+\xi)\exp(-\xi). \tag{3.48}$$

It can satisfy the restrictions at infinity only provided $c_+ = -A\exp(I_+)$, $c_- = A\exp(I_-)$ and $I_+ - I_- = 2\pi i n$, where n is an integer. The latter restriction can be rewritten as

$$\int_s^1 \sqrt{\tilde{k}^2 + m^2/r^2 - (\tilde{\omega} - \tilde{k}M)^2}\,\mathrm{d}r = 2\pi i n, \tag{3.49}$$

where $\tilde{\omega}/\max(M(r)) \leqslant \tilde{k} \leqslant \tilde{\omega}/\min(M(r))$ for $s < r < 1$. Substitution of $\tilde{\omega} = \tilde{k}M(\tilde{r})$ into equation (3.49) gives

$$\int_s^1 \sqrt{1 - (M(\tilde{r}) - M(r))^2\tilde{k}^2 + m^2/r^2}\,\mathrm{d}r = 2\pi i n. \tag{3.50}$$

which is impossible for a subsonic mean flow. Thus, the only possibility is that $\tilde{r} = s$ or $\tilde{r} = 1$. In the first case (3.47) gives way to the following boundary conditions:

$$P(\xi \to +\infty) \to A\xi\left(\mathrm{e}^{-(I_+ + \xi)} + \mathrm{e}^{(I_+ + \xi)}\right) + \cdots, \quad \frac{\mathrm{d}P}{\mathrm{d}\xi}(0) = 0$$

so that $c_+ = -A\exp(I_+)$, $c_- = A\exp(-I_+)$, $\tilde{k} = \tilde{\omega}/M_h$ in the solution (3.48). In the second case the appropriate boundary conditions are

$$P(\xi \to -\infty) \to A\xi\left(\mathrm{e}^{-(I_- + \xi)} + \mathrm{e}^{(I_- + \xi)}\right) + \cdots, \quad \frac{\mathrm{d}P}{\mathrm{d}\xi}(0) = 0,$$

and $c_+ = -A\exp(I_-)$, $c_- = A\exp(-I_-)$, $\tilde{k} = \tilde{\omega}/M_d$, respectively.

Overall, the results of this section show that if the structure of the boundary-layer flow in the immediate vicinity of the duct walls is discarded and the tangential component of the mean flow velocity is assumed non-zero on the walls, then for sufficiently large $\tilde{k}$ there exist two hydrodynamic modes of the Pridmore-Brown equation, with the critical points being exactly on the walls and their phase velocities equal to the mean flow velocity at the walls. This may not be true, however, if the

mean flow velocity has a typical boundary-layer flow profile that satisfies no-slip conditions on the walls.

It is useful to compare the results of this section to the multiple-scale analysis of Golubev & Atassi (1998) obtained for mean flow with solid-body swirl. They demonstrate the existence of a critical layer centred on the purely convective axial wavenumber, where the accumulation of nearly convective eigenvalues takes place for non-zero swirl. Remarkably, if the swirl is set to zero in their dispersion relation (43), the nearly convected modes disappear and the only remaining eigenvalue is the purely convective mode, which is also the case here. Note that clustering of nearly convective modes was reported in Golubev & Atassi (1998) for a differential equation which does not reduce to the Pridmore-Brown equation studied in this section.

4. Conclusions

The propagation of small-amplitude axisymmetric unsteady disturbances in an annular lined duct with mean axial shear flow has been re-examined analytically on the basis of the WKB method. Our emphasis has been on the asymptotic analysis of the high-frequency and short-wavelength modes. This is appropriate in the light of the engineering applications outlined in the Introduction. We have found by means of comparisons with the known exact solution and numerical computations (Vilenski & Rienstra 2006) that the approximation we have derived provides an accurate tool attractive for practical purposes, especially in view of the stiffness of the numerical problem.

The major underlying issue for the proposed study has been whether the mean flow shear and the wall lining significantly influence the properties of the spectrum of the Pridmore-Brown equation.

It follows that the net effect of the mean flow shear on the acoustic part of the spectrum is moderate, and the results found for flows with shear are qualitatively similar to the uniform flow case, provided regions with strong shear gradients are absent. Quantitative differences in the values of modal wavenumbers do arise though. These are illustrated in figure 2 and also in Vilenski & Rienstra (2006), where the evolution of the acoustic modal structure as the main flow changes from the uniform to various parabolic profiles is presented. These differences were found not to be critical from the theoretical standpoint, and for this reason are not discussed here any further.

In contrast, the effect of lining on the acoustic part of the spectrum is of considerable significance. We find that finite resistance on the wall, where the function $q(r)$ from (3.8) is positive, prevents the emergence of the turning points in the flow. As a result, the existence of the related cut-on modes becomes impossible in this case. This is in line with numerical observations (for instance, see figure 3 and also Rienstra 2003*b*) which illustrate the shift of the otherwise cut-on modes off the real axis of the complex plane $\widetilde{k}$, when finite resistance is applied to the suitably chosen wall. Note, though, that the acoustic lining of the opposite wall which lies in the quiet region of the related problem with the hard walls does not have the described effect.

Our analysis also explains the emergence of sinusoidal and circular trajectories in the complex wavenumber plane. Modal wavenumbers follow these trajectories when the reactive part of the wall impedance varies from minus to plus infinity. Circular trajectories (3.19) are typical for the cut-off modes whose mode number n is relatively low, so that the restriction $R \gg \zeta_1 \pi n/\kappa_1$ is satisfied. The sinusoidal eigenvalue contours

(3.25), (3.26) occur when the opposite inequality holds, i.e. for strongly cut-off modes. In both cases explicit prediction of wavenumbers as functions of the frequency, Mach number, wall impedance and tip-to-hub ratio proves to be possible.

In line with the previous numerical findings for the uniform flow case, the problem with a non-uniform mean flow has two surface modes (3.28). Our study shows that their phase speed is proportional to the wall impedance and decreases as the wall Mach number increases.

It is known that mean flow non-uniformity results in the appearance of the hydrodynamic part of the spectrum. The results obtained show that for mean flow profiles with non-zero wall Mach numbers the number of smooth hydrodynamic eigenmodes is finite and they are localized near the duct walls, provided a smoothness condition similar to the classical condition of the Rayleigh inflection-point theorem holds. Unlike its two-dimensional counterpart (Lees & Lin 1946), for axisymmetric flows this condition contains explicit dependence on the streamwise and azimuthal wavenumbers. If the smoothness condition is not satisfied for a given mean flow profile and given wavenumbers, the axial velocity develops a logarithmic singularity at the critical radius, where $\widetilde{k} = \widetilde{\omega}/M(\widetilde{r})$.

However, apart from these modes (whose critical radius coincides with one of the walls), there is a continuum of singular hydrodynamic modes which have a third derivative with a jump at the critical point. These solutions play an important role in construction of the Green's function.

For boundary-layer mean-flow profiles which satisfy the no-slip condition the situation is more complex. Our preliminary computation suggests the existence of a continuous, unbounded hydrodynamic spectrum which arises from the singularity at the critical point (Drazin & Reid 2004). Further analysis of this result is needed.

This work was supported by the "Messiaen" European collaborative project (EU Technical Officer Dietrich Knörzer and Coordinator Jean-Louis Migeot, Free Field Technologies). The present investigations commenced when S. W. R. visited the Department of Applied Mathematics and Theoretical Physics of the University of Cambridge, UK, financed by a grant from the Royal Society. We are very grateful to both the Royal Society, the Department and Professor Nigel Peake for their support, hospitality, inspiring discussions and interest.

REFERENCES

Barantsev, R. G. & Engelgart, V. N. 1987 *Asymptotic Methods in Gas and Fluid Dynamics*, pp. 33–40. Leningrad University Press (in Russian).

Brambley, E. J. & Peake, N. 2006 Surface-waves, stability, and scattering for a lined duct with flow. *AIAA Paper* 2006-2688.

Chapman, C. J. 1994 Sound radiation from a cylindrical duct. Part 1. Ray structure of the duct modes and the external field. *J. Fluid Mech.* **281**, 293–311.

Chapman, C. J. 1996 Sound radiation from a cylindrical duct. Part 2. Source modelling, nil-shielding directions, and the open-to-ducted transfer function. *J. Fluid Mech.* **313**, 367–380.

Cooper, A. J. & Peake, N. 2001 Propagation of unsteady disturbances in slowly varying duct with swirling mean flow. *J. Fluid Mech.* **445**, 207–234.

Cooper, A. J. & Peake, N. 2005 Upstream-radiated rotor-stator interaction noise in mean swirling flow. *J. Fluid Mech.* **532**, 219–250.

Criminale, W. O., Jackson, T. L. & Josine, R. O. 2003 *Theory And Computation of Hydrodynamic Stability*. Cambridge University Press.

Drazin, P. G. & Reid, W. H. 2004 *Hydrodynamic Stability*, 2nd edn. Cambridge University.

Envia, E. 1998 A high frequency model of cascade noise. *AIAA Paper* 98-2318.

Eversman, W. 1991 Theoretical model for duct acoustic propagation and radiation. In *Aeroacoustics of Flight Vehicles: Theory and Practice. Volume 2: Noise Control* (ed. H. H. Hubbard), Chapter 13, pp. 101–163.

Golubev, V. V. & Atassi, H. M. 1998 Acoustic vorticity waves in swirling flows. *J. Sound Vib.* **209**(2), 203–222.

Ingard, K. U. 1959 Influence of fluid motion past a plane boundary on sound reflection, absorption and transmission. *J. Acoust. Soc. Am.* **31**(7), 1035–1036.

Keller, J. B. 1985 Semi-classical mechanics. *SIAM Rev.* **27**(4), 485–504.

Korn, G. A. & Korn, T. A. 1968 *Mathematical Handbook for Scientists And Engineers. Definitions, Theorems And Formulas For Reference And Review* (Second Enlarged And Revised Edn.). McGraw-Hill.

Kousen, K. A. 1999 Eigenmodes of ducted flows with radially-dependent axial and swirl velocity components. *NASA/CR*-1999-208881.

Lees, L. & Lin, C. C. 1946 Investigation of The Stability of The Laminar Boundary Layer in A Compressible Fluid. *NACA Tech. Note.* 1115.

Mattheij, R. M. M., Rienstra, S. W. & ten Thije Boonkkamp, J. H. M. 2005 *Partial Differential Equations: Modeling, Analysis, Computation.* SIAM, Philadelphia.

Myers, M. K. 1980 On the acoustic boundary condition in the presence of flow. *J. Sound Vib.* **71**(3), 429–434.

Naimark, M. A. 1969 *Linear Differential Operators.* Nauka, Moscow.

Nijboer, R. 2001 Eigenvalues and eigenfunctions of ducted swirling flows. *AIAA Paper* 2001-2178.

Ostashev, V. E. 1997 *Acoustics in Moving Inhomogeneous Media.* E & FN Spon.

Ovenden, N. C. 2005 A uniformly valid multiple scales solution for cut-on cut-off transition of sound in flow ducts. *J. Sound Vib.* **286**, 403–416.

Ovenden, N. C. & Rienstra, S. W. 2004 Mode-matching strategies in slowly varying engine ducts. *AIAA J.* **42**, 1832–1840.

Pridmore–Brown, D. C. 1958 Sound Propagation in a fluid flowing through an attenuating duct. *Journal of Fluid Mech.* **4**, 393–406.

Rienstra, S. W. 1999 Sound transmission in slowly varying circular and annular lined ducts with flow. *J. Fluid Mech.* **380**, 279–296.

Rienstra, S. W. 2003*a* Sound propagation in slowly varying lined flow ducts of arbitrary cross-section. *J. Fluid Mech.* **495**, 157–173.

Rienstra, S. W. 2003*b* A classification of duct modes based on surface waves. *Wave Motion* **37**, 119–135.

Rienstra, S. W. 2006 Impedance models in time domain, including the extended Helmholtz resonator model. *12th AIAA/CEAS Aeroacoustics Conference, AIAA Paper* 2006-2686.

Rienstra, S. W. & Tester, B. T. 2005 An analytic Green's function for a lined circular duct containing uniform mean flow. *AIAA Paper* 2005-3020. Revised version submitted to *J. Sound Vib.*

Schlichting, H., Gersten, K., Krause, E., Oertel, H. & Mayers, K. 2000 *Boundary-Layer Theory.* Springer.

Smirnov, V. I. 1981 *A Course of Higher Mathematics,* Volume IV. Nuaka, Moscow (in Russian).

Stakgold, I. 1998 *Green's Functions And Boundary Value Problems.* Wiley-Interscience.

Tam, C. K. W. & Auriault, L. 1998 The wave modes in ducted swirling flows. *J. Fluid Mech.* **371**, 1–20.

Vilenski, G. G. 2006 Mode matching in engine ducts with vortical flows. *AIAA Paper* 2006-2584.

Vilenski, G. G., Rienstra, S. W. 2006 Numerical study of acoustic modes in ducted shear flows. *J. Sound Vib.* (Submitted).

Zorumski, W. E. 1974 Acoustic theory of axisymmetric multi-sectioned ducts. *NASA TR* R-419.